Published in final edited form as:

Cell Rep. 2019 October 08; 29(2): 422–436.e5. doi:10.1016/j.celrep.2019.08.097.

Topoisomerase II Is Crucial for Fork Convergence during Vertebrate Replication Termination

Darren R. Heintzman[1,4], **Lillian V. Campos**[1,4], **Jo Ann W. Byl**[1], **Neil Osheroff**[1,2,3], **James M. Dewar**[1,5,*]

[1]Department of Biochemistry, Vanderbilt University School of Medicine, Nashville, TN 37232, USA

[2]Department of Medicine (Hematology, Oncology), Vanderbilt University School of Medicine, Nashville, TN 37232, USA

[3]VA Tennessee Valley Healthcare System, Nashville, TN 37212, USA

[4]These authors contributed equally

[5]Lead Contact

SUMMARY

Termination of DNA replication occurs when two replication forks converge upon the same stretch of DNA. Resolution of topological stress by topoisomerases is crucial for fork convergence in bacteria and viruses, but it is unclear whether similar mechanisms operate during vertebrate termination. Using *Xenopus* egg extracts, we show that topoisomerase II (Top2) resolves topological stress to prevent converging forks from stalling during termination. Under these conditions, stalling arises due to an inability to unwind the final stretch of DNA ahead of each fork. By promoting fork convergence, Top2 facilitates all downstream events of termination. Converging forks ultimately overcome stalling independently of Top2, indicating that additional mechanisms support fork convergence. Top2 acts throughout replication to prevent the accumulation of topological stress that would otherwise stall converging forks. Thus, termination poses evolutionarily conserved topological problems that can be mitigated by careful execution of the earlier stages of replication.

Graphical Abstract

*Correspondence: james.dewar@vanderbilt.edu.

AUTHOR CONTRIBUTIONS

D.R.H. and L.V.C. performed the experiments. J.A.W.B. and N.O. purified human Top2α. J.M.D. designed the project, with input from D.R.H., L.V.C., and N.O. The manuscript was written by J.M.D. and L.V.C. with input from D.R.H. and N.O.

SUPPLEMENTAL INFORMATION

Supplemental Information can be found online at https://doi.org/10.1016/j.celrep.2019.08.097.

DECLARATION OF INTERESTS

The authors declare no competing interests.

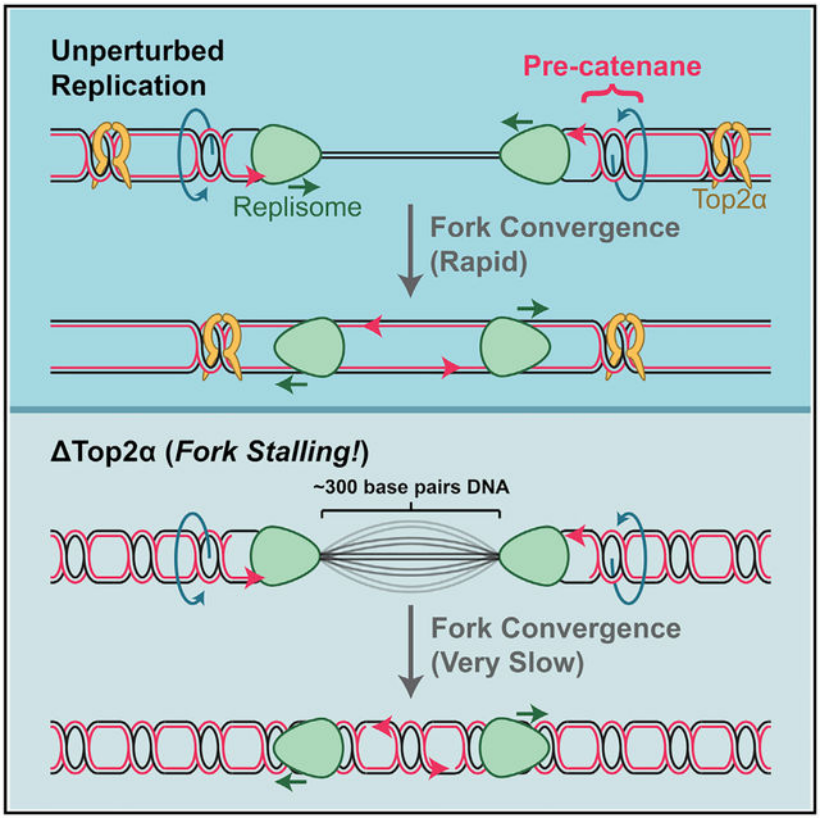

In Brief

To complete DNA synthesis replication, forks must converge on the same stretch of DNA. In vertebrates this process occurs rapidly, but it is unclear which mechanisms support fork convergence. Heintzman et al. find that topoisomerase II promotes fork convergence by preventing accumulation of topological stress earlier during replication.

INTRODUCTION

Eukaryotic DNA replication is carefully orchestrated into discrete steps to ensure faithful duplication of the genome (Bell and Labib, 2016; Bleichert et al., 2017; O'Donnell et al., 2013; Siddiqui et al., 2013; Figure S1). The final stage of replication is called "termination" and occurs when two replication forks converge on the same stretch of DNA (Figures S1 Aiv–S1Aviii). Work in bacteria and viruses has shown that termination poses unique challenges that can result in fork stalling or over-replication of DNA (Hiasa and Marians, 1994; Rudolph et al., 2013; Seidman and Salzman, 1979; Tapper and DePamphilis, 1978). In atypical human cell, approximately 60,000 termination events occur during each S phase (Huberman and Riggs, 1968), and even a single defective termination event could introduce mutations or interfere with mitosis. However, despite the importance of termination, this process is poorly characterized relative to the earlier stages of replication, especially in vertebrates.

Recent studies have begun to shed light on termination and suggest a biochemical model for this process (Dewar and Walter, 2017; Gambus, 2017; Keszthelyi et al., 2016). The onset of termination is believed to occur when converging forks are ~150 base pairs apart, at which point DNA supercoils can no longer be resolved (Figure S1Aiv). As forks advance beyond this point, any topological stress generated by fork movement must be passed behind the forks to generate "pre-catenanes," which are intertwines of double-stranded DNA ("fork convergence," Figures S1Aiv and S1Av) (Champoux and Been, 1980; Schalbetter et al., 2015). Once forks meet, the replisomes rapidly pass each other ("fork merger," Figures S1Av and S1Avi) and move over replicated DNA from the opposing fork (Dewar et al., 2015). This allows nascent strands from one fork to be ligated to the opposing fork ("ligation," Figures S1Avi and S1Avii) (Dewar et al., 2015). At this point, pre-catenanes are now within replicated DNA and are termed "catenanes" (Figure S1Avii) (Ullsperger et al., 1995). Termination ultimately triggers a dedicated replisome removal pathway ("unloading," Figures S1Avii and S1Aviii) that involves ubiquitylation of the replisome by a ubiquitin ligase (SCF^{Dia2} in yeast, $Cul2^{Lrr1}$ in vertebrates) and extraction of the replisome by the AAA+ ATPase p97 (Dewar et al., 2017; Maric et al., 2014; Moreno et al., 2014; Sonneville et al., 2017). Finally, topoisomerase II removes catenanes ("decatenation," Figures S1Avii and S1Aviii) (Baxter and Diffley, 2008; Dewar et al., 2015) to allow chromosomes to separate during mitosis.

In bacteria and viruses, resolution of pre-catenanes by topoisomerase II orthologs is crucial to relieve topological stress so that replication forks can merge (Espeli et al., 2003; Hiasa and Marians, 1996; Ishimi et al., 1992). These enzymes can resolve supercoils, but their unique role during termination is believed to reflect pre-catenane resolution, which cannot be performed by other topoisomerases (Pommier et al., 2016; Vos et al., 2011). In contrast, topoisomerase II plays little role during fork merger in yeast (Baxter and Diffley, 2008; Deegan et al., 2019), and it is unclear whether topoisomerase II promotes fork merger in vertebrates (Cuvier et al., 2008; Gaggioli et al., 2013; Lucas et al., 2001). Thus, topological obstacles to fork merger may be confined to bacteria and viruses.

The topological constraints imposed on converging forks represent the earliest event of termination (Dewar and Walter, 2017; Gambus, 2017; Keszthelyi et al., 2016). However, key mechanistic questions remain about how topological stress influences termination, even in bacteria and viruses. Topological stress is believed to cause a defect in unwinding the final stretch of DNA, but this may instead reflect alterations in fork structure (Ray Chaudhuri et al., 2012; Rudolph et al., 2013). Furthermore, current models propose that pre-catenanes are formed as forks converge (Dewar and Walter, 2017; Gambus, 2017; Keszthelyi et al., 2016), but other work shows that pre-catenanes can form before termination (Lucas et al., 2001; Mariezcurrena and Uhlmann, 2017) and raises the possibility that termination defects arise from earlier stages of replication. It is also unclear how strong the requirement for type II topoisomerases is and to what extent other pathways are sufficient for fork merger (Deegan et al., 2019; Suski and Marians, 2008). Finally, the mechanisms that efficiently target type II topoisomerases to pre-catenanes are unknown. It is important to address these questions to elucidate the mechanism of termination and requirements for this process.

To investigate fork convergence during vertebrate termination, we used *Xenopus* egg extracts to address the role of topoisomerase II. We found that topoisomerase II is crucial for fork progression during termination, and loss of topoisomerase II causes converging forks to stall. Stalling occurs due to a defect in unwinding the final stretch of DNA, rather than altered fork structure or an interaction between opposing replisomes. Forks are ultimately able to terminate even in the absence of topoisomerase II, indicating that additional pathways for fork convergence exist. Topoisomerase II promotes fork merger by acting throughout replication to prevent accumulation of topological stress that would otherwise stall forks during termination. Our data reveal that topological problems posed by vertebrate termination can be mitigated by careful execution of the earlier stages of DNA replication.

RESULTS

Multiple Roles for Top2α during Termination

To begin to address the role of topoisomerase II (Top2) during termination, we first examined whether Top2 is required for decatenation (Figures S1Avii and S1Aviii) as previously described (Baxter and Diffley, 2008; Lucas et al., 2001). To this end, we monitored decatenation during termination of plasmid DNA replication in *Xenopus* egg extracts. In this system (Walter et al., 1998), replication mostly initiates at a single sequence-nonspecific origin to establish two replication forks, which duplicate the remaining plasmid and then readily terminate when they meet (Figure 1A) (Dewar et al., 2017). Top2α was inactivated by immunodepletion, which removed approximately 99% of Top2α from extracts (Figure 1B, lanes 1 and 6). In Top2α-immunodepleted extracts, catenanes persisted and formation of circular monomers was blocked (Figure 1C, lanes 5–8 and 1–4; Figures S1D–S1G), indicating that decatenation was defective (Figures 1D and S1C). This defect was rescued by addition of hTop2α (Figures 1C–1E and S1C). Importantly, there was no discernable impact on the rate or amount of total DNA synthesis (Figure 1F), consistent with previous work (Gaggioli et al., 2013; Lucas et al., 2001). Thus, the absence of circular monomers reflected a defect in termination rather than reduced or slowed initiation or elongation. Our data show that Top2α is required for decatenation, consistent with previous studies.

It is unclear whether Top2α also promotes fork convergence in addition to decatenation (Cuvier et al., 2008; Gaggioli et al., 2013). To test this, we monitored fork merger (Figure 1G), which occurs immediately after fork convergence when the final stretch of parental DNA is disrupted (Figures S1Av and S1Avi). Immunodepletion of Top2α caused double Ys to persist (Figure 1H, lanes 5–8 and 1–4), indicating that fork merger was defective (Figures 1I and S1I). This defect was rescued by addition of hTop2α (Figures 1H, 1I, and S1I). Decatenation and fork merger were rescued at similar concentrations of hTop2α (Figures S1J–S1M), suggesting the same activity was required for both. Top2α immunodepletion did not impact DNA synthesis (Figure 1F) in experiments where fork merger was defective (Figure S1N), indicating a defect in termination and not earlier stages of replication. We conclude that Top2α is important for both decatenation and fork merger during termination of vertebrate DNA synthesis.

Differential Requirements for Fork Merger and Decatenation

Fork merger ultimately went to completion following Top2α-immunodepletion (Figure 1I). We wanted to know whether this was due to residual Top2 activity or Top2-independent pathways (Deegan et al., 2019; Suski and Marians, 2008). To inhibit residual Top2 activity, we immunodepleted Top2α and added the Top2 inhibitor ICRF-193 (Top2-i, Figures 2A–2C and S2B). Top2-i treatment almost completely blocked fork merger (Figures 2B, lanes 5–8 and 1–4, 2C, and S2B). In contrast, Top2-i treatment of Top2α-immunodepleted extracts did not block fork merger (Figures 2B, lanes 9–12 and 13–16, 2C, and S2B). Top2-i caused a much stronger defect than Top2α-depletion (Figure 2B, lanes 5–8 and 9–12), presumably because Top2-i traps Top2 on DNA and exerts dominant-negative effects (Roca et al., 1994). This cannot be due to obstruction of replication forks by trapped Top2 complexes because Top2 only acts behind forks in *Xenopus* egg extracts (Lucas et al., 2001). Further work will be required to determine how trapping Top2 behind forks inhibits fork convergence. Overall, our data show that Top2α is crucial for fork merger, but fork merger can ultimately occur through Top2-independent pathways.

Top2-i inhibits the catalytic activity of Top2 and delayed fork merger, suggesting that Top2 promotes fork merger through resolution of topological stress rather than some non-catalytic role. To test this, we purified catalytically inactive Top2α (Top2α-YF, Figure S2C) and examined its ability to rescue fork merger in Top2α-immunodepleted extracts (Figures S2D and SDE). Although Top2α-YF slowed replication (Figure S2F), it was clear that Top2α-YF enhanced, rather than rescued, the fork merger defect (Figure S2G), consistent with the dominant-negative effect exerted by Top2-i (Figure 2C). Thus, Top2α catalytic activity promotes fork merger, presumably by resolving topological stress.

Immunodepletion of Top2α blocked decatenation (Figure 1D), but catenanes initially formed as a higher mobility species then shifted to a lower-mobility species over time (Figure 1C) suggesting low levels of decatenation. We therefore tested whether decatenation could proceed independently of Top2, as observed for fork merger. To address whether the mobility shift was also independent of Top2, as observed for fork merger, we treated Top2α-immunodepleted extracts with Top2-i (Figures 2D and 2E). Interestingly, Top2-i treatment blocked the shift from high mobility (Cats+, Figure 2E) to low mobility (Cats−, Figure 2E) species (Figures 2E, compare lanes 13–16 to 9–12, 2F, and S2I–S2K). Pulse-chase analysis confirmed that fork merger initially produced Cats+, which were converted to Cats− (Figure S2L) but did not yield circular monomers, due to the decatenation defect (Figure 1D). Although Cats+ superficially resembled Φ structures, which are formed following catalytic inhibition of Top2 in yeast (Baxter and Diffley, 2008), both Cats+ and Cats− were distinct from Φs (Figures S3A–S3C). Formation of Cats− was also blocked by the Top2-inhibitor Merbarone (Figures S3D–S3I), further suggesting that Cats− arose from partial decatenation of Cats+. To test this, we immunodepleted Top2α and performed 2D gel electrophoresis to measure the number of linkages within the catenanes in the absence or presence of Top2-i (Figure 2G). At 30 min, ~18 linkages were present (≥20 linkages in Figures 2Hii and 2I; ~15 linkages in Figure S4M), but this was reduced to ~5 by 180 min (~8 linkages in Figures 2Hiii and 2I; ~2 linkages in Figure S4M), indicating that residual decatenation took place. In the presence of Top2-I, ≥ 20 linkages were present at both 30 min and 180 min (Figures

2Hv, 2Hvi, 2J, and S4N), demonstrating that the residual decatenation was due to Top2. Top2-i is likely to block residual decatenation by inhibiting Top2β, which is also present in extracts (Wühr et al., 2015). However, we have so far been unable to generate a functional Top2β antibody to test this. Overall, our data show that fork merger can occur independently of Top2, but decatenation cannot.

Top2α Is Crucial for Fork Convergence

To address the cause of the fork merger defect we observed, we first tested whether topological stress during termination caused fork reversal, as previously proposed (Ray Chaudhuri et al., 2012; Rudolph et al., 2013). To this end, we analyzed replication intermediates from Top2α-immunodepleted extracts by 2D gel electrophoresis (Figure 3A). Immunodepletion of Top2α caused replication intermediates to persist, consistent with a retention of replication forks on DNA (Figures 3Bv–3Bviii and 3Bi–3Biv). In both mock- and Top2α-immunodepleted extracts, the same double Y-, bubble-, and X-shaped intermediates were retained, indicating that fork structure was mostly unaltered (Figures 3A, 3Bi, and 3Bv). Top2α immunodepletion also led to formation of Y structures (Figures 3Bi, 3Bii, 3Bv, and 3Bvi), indicating that loss of Top2α caused fork breakage (Figure S4B). However, these structures were of low abundance. Thus, in the majority of cases, impaired fork convergence is not attributable to fork reversal or any other alterations in fork structure.

The fork merger defect could arise due to collision between opposing replisomes (Figure S1Av). Alternatively, topological stress might prevent the final stretch of DNA from being unwound, resulting in stalling during the earlier fork convergence step (Figure S1Aiv). To distinguish these possibilities, we sought to measure the amount of unreplicated DNA between the stalled forks, since a collision between replisomes should result in almost completely replicated molecules, while a defect in unwinding the final stretch of DNA should result in significant unreplicated DNA between the two forks. To this end, we monitored the replication intermediates formed in mock- and Top2α-immunodepleted extracts by denaturing gel analysis (Figure 3C). The predicted species are stalled nascent strands (SNS, Figure 3C), double-stranded monomers (dsMs, Figure 3C), and catenated dimers (Cats, Figure 3C). To identify the stalled nascent strands, we also treated the same samples with a nicking enzyme (Figure 3D), which should alter the structure of the double-stranded monomers (resulting in single-stranded monomers and replicated nicked molecules; Figure 3D) and catenated dimers (resulting in hemicatenated dimers and replicated nicked molecules; Figure 3D), while leaving half of the stalled nascent strands intact (SNS, Figure 3D). As expected, nicking increased the mobility of double-stranded monomers (Figure 3E, compare lanes 15–18 and 2–5) as the resultant single-stranded monomers were half the size (3,402 in Figure 3D versus 6,804 in Figure 3C). Surprisingly, nicking reduced the mobility of catenated dimers (Figure 3E, compare lanes 20–22 and 7–9) even though the resultant hemicatenated dimers were half the size (6,804 in Figure 3D versus 13,608 in Figure 3C). The decreased mobility of hemicatenated dimers is likely to reflect a less compact DNA structure (in the catenanes, each DNA strand is wrapped around three other strands, while in the hemicatenanes each strand is only wrapped around one other strand). Importantly, nicking left a subpopulation of stalled nascent strands unaffected (Figure 3E, compare lanes 19 and 6). We confirmed the identity of these species by treatment with recombinant

hTop2α and monitoring fork convergence (Figures S4D and S4E). We then analyzed the size of stalled nascent strands alongside a DNA ladder that corresponded to different amounts of unreplicated DNA (Figure 3E, lanes 10–14) and found that on average ~360 nucleotides of unreplicated DNA remained (Figures 3F and S4H–S4K). Because each replisome has a footprint of approximately 60 nucleotides on both strands (Dewar et al., 2015), these data indicate that ~300 bp of unreplicated DNA remains between the two stalled forks (Figure 3F). Thus, Top2α promotes fork convergence, most likely by facilitating unwinding of the final stretch of DNA between the two forks.

Our data show that Top2α is crucial for replisomes to unwind the final ~300 bp of DNA when an opposing replisome is encountered. We wanted to know whether this requirement was unique to converging replication forks or reflected a more general role for Top2α in facilitating DNA unwinding ahead of replication forks. To address this issue, we examined whether Top2α was important for replication forks to approach a LacR array (Figure 3G), which blocks replication (Dewar et al., 2015). We immunodepleted Top2α and replicated plasmid DNA containing a LacR array, then separated replication intermediates on a denaturing agarose gel. Replication intermediates were nicked to allow us to monitor leading strands approaching one edge of the LacR array (LS, Figure 3G). Following mock-immunodepletion, we observed a collection of nascent products that arose from forks stalled at the LacR array (Figure 3H, NS ~2,658), and these products were ~300 nucleotides shorter in Top2α-immunodepleted extracts, indicating that forks were unable to approach the LacR array (Figures 3H, nascent < 2,658, 3I, and S4L–S4Q). Mock-immunodepleted nascent strands slowly progressed through the LacR array, while Top2α-immunodepleted nascent strands remained ~300 nucleotides shorter at all time points (Figure 3I). Top2α-immunodepletion prevented ~80% of leading strands from encountering the LacR array (Figure 3J), indicating that each fork stalled ~150 base pairs away from the LacR array. Thus, the requirement for Top2α during termination reflects a more general role in allowing the final ~150 base pairs ahead of a replication fork to be unwound.

Stalling Does Not Alter the Mechanism of Termination

During termination, ligation rapidly follows fork merger and replisomes are unloaded after forks merge (Figures S1Aiv–S1Aviii). In contrast, fork stalling can activate DNA repair pathways that uncouple ligation from fork merger and unload the replisome before forks merge (Wu et al., 2019). To address whether stalling affected the mechanism of termination, we first tested whether ligation was uncoupled from fork merger. To this end, we immunodepleted Top2α and monitored ligation (Figure 4A). Immunodepletion of Top2α delayed the formation of full-length strands, indicating that ligation was defective (Figures 4B, lanes 5–8 and 1–4,4C, and S5B). This defect was rescued by re-addition of recombinant hTop2α (Figures 4B, lanes 9–12 and 5–8, 4C, and S5B). When we analyzed ligation and fork merger across multiple experiments (Figure 4D), we found that ligation occurred with almost identical kinetics to fork merger in both mock- and Top2α-immunodepleted extracts. Thus, ligation remains tightly coupled to fork merger following immunodepletion of Top2α. Furthermore, Top2α is crucial for ligation, presumably due to its role in promoting fork merger.

We next tested whether replisomes are unloaded after ligation, as observed during termination (Dewar et al., 2015), or prior to ligation, as observed during stalled fork responses (Wu et al., 2019). To this end, we immunodepleted Top2α and performed plasmid pull-downs to recover chromatin-bound proteins (Figure 4E), which were then analyzed by western blotting (Figure 4F). Immunodepletion of Top2α caused the replisome proteins MCM6 and CDC45 to persist (Figures 4F, compare lanes 7–10 and 2–5, 4G, and 4H), indicating that replisome unloading was defective. The replisome unloading defect was rescued by addition of hTop2α (Figures 4F, compare lanes 12–15 and 7–10, 4G, 4H, S5C, and S5D). Importantly, MCM6 and CDC45 dissociated with similar kinetics to RPA70 and RPA30 (Figures 4F, compare lanes 7–10 and 2–5, 4G–4J, and S5C–S5F), whose dissociation acts as a readout for ligation (Dewar et al., 2015), suggesting that replisome unloading did not occur prior to ligation. To further test whether replisome unloading occurred before or after fork merger, we immunodepleted Top2α and added the p97 inhibitor NMS-873, which blocks all known replisome unloading pathways (Figures S5I–S5M) (Wu et al., 2019). However, NMS-873 treatment had no effect on fork merger (Figures S5I–S5M). Thus, replisome unloading does not appear to occur before ligation and is not required for fork merger, as is normally the case during termination (Dewar et al., 2015). These data suggest that once forks merge, ligation and replisome unloading occur using the same mechanism that normally operates during termination. Furthermore, as a result of its role during fork merger, Top2α is crucial for both ligation and replisome unloading.

Top2α Activity throughout Replication Promotes Termination

Type II topoisomerases are required for fork merger in bacteria and viruses (Hiasa and Marians, 1996; Ishimi et al., 1992). The requirement for these topoisomerases is believed to reflect their role during termination and not at earlier stages of replication, but this is untested (Dewar and Walter, 2017; Gambus, 2017; Keszthelyi et al., 2016), and other work shows that pre-catenanes can form prior to termination (Lucas et al., 2001; Mariezcurrena and Uhlmann, 2017). We therefore decided to address whether the requirement for Top2α during fork merger reflected its role during termination or at earlier stages of replication. To address this, we used Top2-i to inhibit Top2 either throughout replication or only during termination. To this end, we replicated plasmid DNA containing a LacR-bound 32x*lacO* array and then added Top2-i at 6 min so that Top2-i was present throughout most of replication or at 18 min so that Top2-i was present primarily during termination (Figure S6A). We then added isopropyl β-D-1-thiogalactopyranoside (IPTG) at 20 min to induce termination and monitored fork merger in all conditions (Figures S6B and S6C). DNA synthesis was ~30% complete at 6 min, which corresponded to early addition of Top2-i, while DNA synthesis was ~80% complete by 18 min, which corresponded to late addition of Top2-I (Figure S6D). Additionally, the signal plateaued by 12 min, indicating that forks were all stalled at the LacR array by this point (Figure S6D). Early addition of Top2-i delayed fork merger by ~50 min compared to the vehicle, while late addition of Top2-i delayed fork merger by ~2 min compared to the vehicle (Figure S6E). These results were complicated by the fact that inclusion of Top2-i throughout replication appeared to activate a DNA repair pathway that converted double Ys to aberrant replication intermediates (ARIs) (Deng et al., 2018) at later time points (lanes 13 and 14 of Figure S6B). However, the difference in fork merger was observed prior to ARI formation (lanes 10–12, Figures S6B

and S6C; 20–35 min, Figure S6E), so formation of ARIs does not impact our assessment of fork merger. We also performed additional controls to ensure that our conclusions were not influenced by stalling forks in the presence of Top2-i (Figures S6F–S6J) or the length of time for which Top2-i was present (Figures S6K–S6O). Overall, our data argue that Top2α acts throughout replication to promote fork merger.

A caveat of the experiments shown in Figures S6A–S6M is that Top2-i exerts dominant-negative effects (Figure 2), which could, in principle, cause us to overestimate the role of Top2 outside of termination. To more accurately assess the role of Top2 outside of termination, we developed an alternate strategy to inhibit Top2α throughout replication or only during termination (Figure 5A). To inhibit Top2α throughout replication, we monitored fork merger in mock- and Top2α-immunodepleted extracts ("Top2α immunodepletion," Figure 5A). To inhibit Top2α during termination, we stalled forks at a LacR array in mock-immunodepleted extracts, then induced termination in the absence or presence of Top2-i ("Top2-i treatment," Figure 5A). This approach causes the *termination role* of Top2α to be *overestimated*, while accurately assessing the role of Top2α throughout replication. In Top2α-immunodepleted extracts, fork merger was delayed by ~30 min compared to mock-immunodepleted extracts (Figures 5B, lanes 1–4 and 5–8, 5C, and S6Q). However, in Top2-i treated extracts, fork merger was delayed by ~5 min (Figures 5B, lanes 10–13 and 14–17, 5D, and S6R). These data show that inhibition of Top2α during termination results in much weaker fork merger defect than inhibition of Top2α throughout replication, even under conditions where the termination role of Top2α is overestimated. Although forks were only stalled at a LacR array in the presence of Top2-i (Figure 6D) and not following Top2α immunodepletion (Figure 5C), this does not impact our conclusions as the same results were observed when forks were stalled at a LacR array in all conditions (Figures S6F–S6H and S6K–S6M). Overall, these data support a model where Top2α resolves topological stress throughout replication to prevent accumulation of topological stress from stalling forks during termination.

We next wanted to know whether the role of Top2α throughout replication reflected resolution of pre-catenanes, which are expected to be rare during earlier stages of replication. To address this, we inhibited Top2α either throughout replication or only during termination using the same strategy described above (Figure 5A) and then analyzed the catenanes formed (Figure 5E). Top2α-immunodepleted extracts predominantly formed the highly catenated Cats+ species (Figure 5F, lane 8) as described above (Figure 2). In contrast, Top2-i treated extracts predominantly formed the less catenated Cats− species (Figure 5F, lanes 15–17). Importantly, decatenation was blocked by both interventions (Figures 5G, 5H, S6T, and S6U). Thus, inhibition of Top2α during termination resulted in less catenated linkages than inhibition of Top2α throughout replication. These data indicate that Top2α resolves pre-catenanes throughout replication to promote termination.

Top2α Binds DNA throughout Replication

Our data indicate that Top2α resolves pre-catenanes throughout replication to promote fork merger. We therefore wanted to know how recruitment of Top2α is coordinated to allow rapid termination of DNA synthesis under normal conditions (Dewar et al., 2015). We first

tested whether Top2α binding is replication dependent. To this end, we treated extracts with the Cdc7 inhibitor PHA-767491 (Cdc7-i) to block replisome activation (Montagnoli et al., 2008) or Geminin to block replisome loading (Wohlschlegel et al., 2000) (Figure 6A) and used plasmid pull-downs to monitor association of Top2α and other replisome proteins to DNA (Figure 6B). As expected, Cdc7-i blocked binding of CDC45 but not MCM6 (Figure 6B, lanes 8–12 and 3–7), while Geminin blocked binding of both CDC45 and MCM6 (Figure 6B, lanes 13–17 and 3–7). Both Cdc7-i and Geminin blocked DNA replication, as evidenced by dramatically reduced levels of the replication fork proteins RPA and PCNA compared to the mock (Figure 6B). Interestingly, Top2α binding was strongly reduced by both Cdc7-i and Geminin treatment (Figure 6B). Thus, Top2α binding was strongly replication dependent. Top2α levels were slightly higher in the presence of Geminin than Cdc7-i (Figure 6B, lanes 8–12 and 13–17), which may reflect the previously-described interaction between Top2α and Geminin (Gardner et al., 2011). Top2α levels were high at early time points and gradually decreased over time but persisted beyond 30 min (Figures 6C and S7A). In contrast, RPA, PCNA, and CDC45 all dissociated much sooner (Figures 6D and S7B). These data show that Top2α exhibits replication-dependent binding that persists after other replication proteins dissociate from DNA.

Current models propose that pre-catenanes are formed during termination and resolved by Top2 (Dewar and Walter, 2017; Gambus, 2017; Keszthelyi et al., 2016), which should result in heightened Top2 binding during termination. In contrast, our data suggest that Top2 plays a major role throughout replication, which should result in high levels of Top2 binding prior to termination. To test whether Top2α binds prior to termination, we replicated plasmid DNA containing a LacR array, added IPTG to permit termination or withheld IPTG to block termination, then monitored DNA binding of Top2α and other replication proteins by plasmid pull-downs. CDC45, MCM6, RPA, and PCNA persisted on DNA when IPTG was withheld (Figures 6F, lanes 8–11, 6G–6I, and S7C–S7E) but dissociated when IPTG was added (Figures 6F, lanes 3–6, 6G–6I, and S7C–S7E), indicating that termination was efficiently blocked by the LacR array and induced by IPTG addition. Top2α binding was readily detected at early time points and was reduced when IPTG was added (Figures 6J, lanes 8–11 to 3–6, 6G, and S7F). Therefore, Top2α binding occurs prior to termination and Top2α does not appear to be recruited to DNA during termination. The same conclusion was reached when we synchronously induced termination and performed a fine time course of Top2α binding (Figures S7J–S7L). Additionally, early Top2α binding did not reflect constitutive association with the replisome (Figure S7M), as previously reported (Sonneville et al., 2017). Overall, these data support our model that Top2α binds throughout replication to promote fork merger.

Finally, we wanted to test whether early binding of Top2α reflects its recruitment to pre-catenanes or supercoils, which can be directly recognized by purified Top2α (McClendon et al., 2005). To this end, we replicated plasmid DNA in the absence or presence of aphidicolin, which blocks DNA synthesis but not unwinding (Walter and Newport, 2000) and results in extensive supercoil generation ahead of forks (Walter and Newport, 2000) but blocks pre-catenane generation behind forks (Figure S7N). Plasmid pull-downs revealed dramatic accumulation of RPA, indicating extensive unwinding (Figures 6L, lanes 9–13 and 3–8, 6M, and S7O). However, Top2α binding was completely blocked by aphidicolin

(Figures 6L, compare lanes 9–13 to 3–8, 6N, and S7P). This could not be attributed to altered levels of replisome activation, as similar levels CDC45 were present on chromatin at early time points (Figure 6L, lanes 10 and 11 and 4 and 5; Figure S7Q). Thus, early Top2α binding reflects its recruitment to pre-catenanes but not supercoils.

DISCUSSION

How Top2α Shapes Termination

Fork convergence during vertebrate termination is rapid and does not involve detectable stalling or slowing of replication (Dewar et al., 2015). We now report that rapid fork convergence is achieved through resolution of pre-catenanes by Top2α (Figure 7A). Although Top2α resolves pre-catenanes throughout replication (Figure 5F), this only becomes important during fork convergence (Figures 5C and 5D), suggesting that terminating forks are particularly sensitive to topological stress. It is formally possible that Top2β is co-depleted with Top2α and fulfills the same role. However, we rescue the fork merger defect with recombinant Top2α (Figure 1I), which definitively demonstrates a role for Top2α in fork convergence.

In our model (Figure 7A), Top2α prevents accumulation of topological stress that would otherwise stall forks during termination (Figure 7B). This implies that pre-catenanes must be rapidly recognized and resolved by Top2α to prevent fork stalling during termination. Our data suggest a simple model for how pre-catenanes are rapidly recognized. Top2α binds pre-catenanes at early time points and persists on chromatin long after termination is complete (Figure 6). The persistent binding of Top2α may allow pre-catenanes to be readily captured and resolved as they diffuse within the replicated region of DNA (Figure 7A), obviating the need to recruit Top2α to individual pre-catenanes. It will be important to test how Top2α is retained on DNA and whether this promotes rapid fork convergence.

Replication forks are ultimately able to merge even in the absence of Top2 activity (Figures 2A–2C, 7Bi, and 7Bii), indicating that additional mechanisms help forks merge. One possibility is that the replisome itself can overcome stalling, given the ability of the replisome to bypass stalling lesions (Sparks et al., 2019). Another possibility is that topoisomerase I can compensate for loss of Top2, since both enzymes cooperate during replication elongation (Bermejo et al., 2007; Brill et al., 1987). Alternatively, topoisomerase IIIα or topoisomerase IIIβ may be able to resolve topological stress, as observed for the bacterial ortholog (Lee et al., 2019; Suski and Marians, 2008). Finally, $5'-3'$ helicases may help forks merge, as observed in yeast (Deegan et al., 2019; Ivessa et al., 2000). Thus, redundant mechanisms may contribute to rapid fork merger during termination. Even though fork merger can occur independently of Top2, the ~20-min delay we observe would likely to be a significant obstacle to genome stability because ~60,000 termination events are required to synthesize the genome of a human cell.

Once forks merge, the downstream events of ligation and replisome unloading proceed to completion (Figure 4). It is likely that ligation and replisome unloading occur using the same mechanism that is normally employed during termination, because ligation and replisome unloading quickly follow fork merger, and replisome unloading is not required for DNA

synthesis, as previously described (Dewar et al., 2015) (Figures 7Aiii–7Av). Overall, loss of Top2α causes converging forks to stall without altering the downstream events of termination, indicating that the mechanism of termination is robust enough to withstand fork stalling.

Requirements for Top2 during Termination

Previous studies reached conflicting conclusions about the role of Top2 during vertebrate termination (Cuvier et al., 2008; Gaggioli et al., 2013; Lucas et al., 2001). Our data show that loss of Top2α causes forks to stall during termination (consistent with Cuvier et al., 2008) but also that forks are ultimately able to complete DNA synthesis (consistent with Gaggioli et al., 2013). Thus, our study indicates that resolution of topological stress promotes fork convergence during vertebrate termination, as observed in bacteria and viruses (Hiasa and Marians, 1996; Ishimi et al., 1992). Although a previous study showed that pre-catenanes can form outside of termination (Lucas et al., 2001), no effect on fork progression or convergence was observed. In contrast, our data show that resolution of catenanes throughout replication is important for fork convergence. This is different to current models where catenanes are only formed during termination (Bell and Labib, 2016; Dewar and Walter, 2017; Gambus, 2017; Keszthelyi et al., 2016). Overall, our data suggest that fork convergence may be targeted by chemotherapeutics that inhibit Top2 (Nitiss, 2009).

Studies in yeast showed that loss of Top2 has little effect on completion of DNA synthesis (Baxter and Diffley, 2008; Deegan et al., 2019). Thus, loss of Top2 in vertebrates appears to impact termination much more strongly than in yeast. This difference cannot be explained by our use of circular minichromosome templates (Figure 1A) because similarly sized circular minichromosomes were also used in the yeast studies (Baxter and Diffley, 2008; Deegan et al., 2019). Instead, the difference may be explained by the extent of pre-catenane generation in vertebrates compared to yeast. Indeed, pre-catenane generation is regulated in yeast and restricted to specific situations, such as termination (Schalbetter et al., 2015). In contrast, pre-catenanes appear to be formed throughout replication in vertebrates (Figures 5 and 6). This distinction suggests that there are mechanistic differences between yeast and vertebrate termination. Accordingly, replisome unloading proceeds through a single pathway during termination in yeast (Maric et al., 2014), while multiple pathways cooperate to unload the replisome during vertebrate termination (Sonneville et al., 2017). It will be interesting to address whether there are fundamental differences in termination between yeast and vertebrates.

A potential pitfall of our approach is that circular minichromosomes may behave differently to full-length linear chromosomes during DNA replication. Importantly, topoisomerases are required for DNA synthesis on circular minichromosomes (Yeeles et al., 2015) just like full-length linear chromosomes (Bermejo et al., 2007; Brill et al., 1987) but unlike linear minichromosomes (Yeeles et al., 2015). Thus, circular minichromosomes experience similar topological issues to long linear chromosomes in a nucleus. However, circular minichromosomes in *Xenopus* egg extracts primarily utilize a single origin of replication (Figures S7J–S7L) in contrast to linear chromosomes, which utilize thousands of origins (Huberman and Riggs, 1968). Additionally, replication of minichromosomes in *Xenopus* egg

extracts occurs without a nucleus (Walter et al., 1998), without transcription (Wang and Shechter, 2016), and on templates too small to support topologically associating domains (Rowley and Corces, 2018). It will therefore be interesting to address whether these additional features exacerbate or ameliorate the requirement for Top2 during fork convergence.

The Trigger for Termination

Our data raise important questions about how termination is triggered in vertebrates. Current models propose that termination begins when converging forks generate pre-catenanes because the intervening DNA becomes too short for supercoils to be resolved (Figure S1iv) (Dewar and Walter, 2017; Gambus, 2017; Keszthelyi et al., 2016). However, our data argue that pre-catenanes are formed and resolved throughout replication by Top2α (Figures 7Ai and 7Aii), consistent with other studies (Lucas et al., 2001; Mariezcurrena and Uhlmann, 2017). Therefore, pre-catenane generation is not specific to termination in vertebrates. Instead, our data suggest that the earliest stage of termination is when forks are ~300 bp apart (Figure 3F), when Top2α becomes crucial to unwind the remaining DNA and fork progression becomes sensitive to topological stress (Figure 1I). Top2α is also crucial to unwind the final ~150 bp of DNA adjacent to a LacR array (Figure 3I). Thus, the requirement for Top2α reflects problems with unwinding the final stretch of DNA, rather than an interaction between opposing replication forks. Previous studies of SV40 replication showed that Top2 is crucial for termination on chromatin but not naked DNA template (Ishimi et al., 1992). We therefore speculate that chromatin poses an obstacle to unwinding the final stretch of DNA. One possibility is that nucleosomes exclude Top1 from the final stretch of DNA or prevent supercoil formation and thus require pre-catenane resolution to relieve topological stress, as proposed in current models. Alternatively, pre-catenane resolution may be crucial to displace the final nucleosomes. However, further work will be required to elucidate the challenges posed by unwinding the final stretch of DNA and how they are solved by Top2.

STAR★METHODS

LEAD CONTACT AND MATERIALS AVAILABILITY

Further information and requests for resources and reagents should be directed to and will be fulfilled by the Lead Contact, James Dewar (james.dewar@vanderbilt.edu). Antibodies generated in this study are available without restriction upon request. No other unique reagents were generated.

EXPERIMENTAL MODEL AND SUBJECT DETAILS

Xenopus laevis—Egg extracts were prepared using *Xenopus laevis* (Nasco #LM0053MX, LM00715MX). All experiments involving animals were approved by the Vanderbilt University International Animal Care and Use Committee.

METHOD DETAILS

Xenopus egg extracts—*Xenopus* egg extracts were prepared from *Xenopus laevis* wild-type males and females (Nasco) as previously described (Lebofsky et al., 2009) and summarized briefly below.

To prepare Crude Interphase Extract (CIE), 6–18 female frogs were each injected with 80 IU of human chorionic gonadotrophin (HCG). 2–7 days later, frogs were injected with 625 IU of HCG to induce egg laying and housed individually in 100 mM NaCl. 20–22 hours later, eggs from each frog were inspected and batches containing high quality (< 5% aberrant morphology) eggs were pooled. Eggs were then stirred in L-cysteine buffer (2.2% cysteine-HCl, pH7.7) for 8 minutes, washed 3 times with 0.5X MMR buffer (50 mM NaCl, 1 mM KCl, 0.25 mM $MgSO_4$, 1.25 mM $CaCl_2$, 2.5 mM HEPES, 0.05 mM EDTA, pH 7.8), and washed 3 times with Egg Lysis Buffer (250 mM Sucrose, 2.5 mM $MgCl_2$, 50 mM KCl, 1 mM DTT, 50 μg/ml cycloheximide, 10 mM HEPES pH7.7). Eggs were then allowed to settle, and supernatant was discarded. Eggs were concentrated by centrifugation at 176 × g for 1 minute and any remaining supernatant was discarded. Eggs were then supplemented with cytochalasin B (final concentration: 2.5 μg/ml), aprotinin (5 μg/ml), and leupeptin (5 μg/ml) before being lysed by centrifugation at 20,000 × g in a swinging bucket rotor at 4°C for 20 minutes. CIE was recovered with a needle and syringe then stored on ice.

To prepare High Speed Supernatant (HSS), 4–20 mL of CIE was supplemented with cycloheximide (final concentration: 50 μg/ml), DTT (final concentration: 1 mM), cytochalasin B (final concentration: 2.5 μg/ml), aprotinin (final concentration: 5 μg/ml), and leupeptin (final concentration: 5 μg/ml) then centrifuged at 260,000 × g in a swinging bucket rotor at 2°C for 33 minutes. Following centrifugation, lipids were aspirated and the soluble HSS was recovered, frozen in liquid nitrogen, then at stored at −80°C.

To prepare NucleoPlasmic Extract (NPE), 30–50 mL of CIE was supplemented with cycloheximide (final concentration: 50 μg/ml), DTT (final concentration: 1 mM), cytochalasin B (final concentration: 2.5 μg/ml), aprotinin (final concentration: 5 μg/ml), leupeptin (final concentration: 5 μg/ml), and nocodazole (final concentration: 3.3 μg/ml) then centrifuged at 20,000 × g in a swinging bucket rotor at 4°C for 10 minutes. Following centrifugation, lipids were aspirated and the remaining CIE was collected while leaving behind the membranous pellet that formed during centrifugation. CIE was then supplemented with creatine phosphokinase (final concentration: 5 μg/ml), phosphocreatine (final concentration: 20mM), and ATP (Final concentration: 2 mM) then incubated at room temperature for 5 minutes. Nuclear assembly was initiated by addition of demembranated sperm chromatin (final concentration: 4,400 sperm/μl) and proceeded for 60–90 minutes at room temperature with end-over-end rotation. Nuclear assembly reactions were then centrifuged at 20,000 × g in a swinging bucket rotor at 4° C for 2 minutes. The nucleoplasmic layer was recovered then centrifuged at 260,000 × g in a swinging bucket rotor at 4°C for 30 minutes. Following centrifugation, lipids were aspirated and the soluble NPE was recovered, frozen in liquid nitrogen, then at stored at −80°C.

DNA replication in Xenopus egg extracts—Unless otherwise stated in the figure legend, all experiments were performed at least twice and a representative result is shown.

All quantifications are either ≥ 3 repeats with error bars or a biological replicate is shown in the supplemental data. All experimental repeats reflect independently-assembled reactions that constitute biological replicates.

Licensing mix was prepared by incubating 0.1 volumes of DNA (final concentration: 15 ng/μl) with 0.9 volumes of High Speed Supernatant (HSS) supplemented with nocodazole (final concentration: 3ng/μl) and ATP regenerating system (ARS, final concentration: 20mM phosphocreatine, 2 mM ATP, 5 ng/μl creatine phosphokinase) for 30 minutes at room temperature. Nucleoplasmic extract (NPE) was activated by adding DTT (final concentration: 2 mM) and ARS. Where DNA was radiolabeled, NPE was also supplemented with [α-^{32}P]dATP (final concentration: 100–360 nM). NPE mix was made by combining 1 volume NPE with 1 volume Egg Lysis Buffer (ELB, 250 mM Sucrose, 2.5 mM $MgCl_2$, 50 mM KCl, 10 mM HEPES pH7.7). Replication was initiated by adding 2 volumes NPE mix to 1 volume Licensing mix. Reactions were stopped by addition of 10 volumes Stop Solution (0.5% SDS, 25 mM EDTA, 50 mM Tris-HCl pH7.5), and treated with RNase A (final concentration: 190 ng/μl) then Proteinase K (909 ng/μl). Stopped reactions were then either directly analyzed by gel electrophoresis or purified, as previously described (Dewar et al., 2015), and subjected to termination assays or 2-D gels.

Top2-i (ICRF-193, Sigma) was dissolved in DMSO and added to reactions at a final concentration of 200 μM. Merbarone was dissolved in DMSO and added to reactions at a final concentration of 100 μM. Cdc7-i (PHA-767491, Sigma) was dissolved in water and incubated with NPE mix at 300 μM for at least 10 minutes before initiating replication. Geminin was dissolved in ELB and incubated with HSS at 10 μM for at least 10 minutes before licensing. In all cases the vehicle control was the same solvent that the agent was dissolved in. Where DMSO was the solvent, it was added to reactions at a final concentration of 4% (V/V).

Protein purification—Human topoisomerase IIα was expressed and purified as described previously (Elsea et al., 1995; Kingma et al., 1997; Worland and Wang, 1989). Briefly, topoisomerase IIα was purified from *Saccharomyces cerevisiae* (DBY745) containing the human TOP2A gene in the inducible overexpression plasmid YEpTOP2-pGAL1. Alternatively the TOP2A-Y805F mutant was expressed from YEpTOP2Y805F-pGAL1. All steps were carried out at 4°C. Cells were lysed, and topoisomerase IIα was extracted from chromosomes that were precipitated with polymin P. Following differential precipitation with $(NH_4)_2SO_4$, the pellet containing topoisomerase IIα was resuspended, applied to, and eluted from a hydroxylapatite column. Fractions containing human topoisomerase IIα (as monitored by gel electrophoresis) were collected, diluted and concentrated by applying it to a phosphocellulose collection column and batch eluting the protein. Fractions containing topoisomerase IIα were pooled, aliquoted, frozen in liquid nitrogen and stored at −80°C.

Biotinylated LacR was expressed in *Escherichia coli* (T7 express) and purified as described previously (Dewar et al., 2015). Briefly, cell pellets were resuspended in lysis buffer (50 mM Tris-HCl, pH 7.5, 5 mM EDTA, 100 mM NaCl, 1 mM DTT, 10% sucrose (w/v), cOmplete protease inhibitor (Roche, Nutley, NJ). The cells were lysed at room temperature in the presence of 0.2 mg/ml lysozyme and 0.1% Brij 58. The insoluble, chromatin-containing

fraction was isolated by centrifugation at 4°C. Chromatin-bound LacR was then released by sonication (in 50 mM Tris-HCl, pH 7.5, 5 mM EDTA, 1 M NaCl, 1 mM DTT, cOmplete protease inhibitor, 30 mM IPTG). DNA was removed from the soluble fraction by addition of polymin P (final concentration 1%), LacR was precipitated by addition of ammonium sulfate (final concentration 37%). The precipitate was dissolved in wash buffer (50 mM Tris-HCl, pH 7.5, 1 mM EDTA, 2.5 M NaCl, 1 mM DTT, cOmplete protease inhibitor) and then applied to a column of SoftLink avidin resin (Promega, Madison, WI). LacR was eluted (in 50 mM Tris-HCl, pH 7.5, 1 mM EDTA, 100 mM NaCl, 1 mM DTT, 5 mM biotin) and dialyzed overnight (against 50 mM Tris-HCl, pH 7.5, 1 mM EDTA, 150 mM NaCl, 1 mM DTT, 38% glycerol (v/v)). Purified LacR was frozen in liquid nitrogen and stored at −80°C.

Antibodies—Antibodies recognizing Cdc45, Mcm6, RPA, and PCNA were previously-described (Dewar et al., 2017; Semlow et al., 2016). Anti-Top2α was raised against a peptide of CAQAGRQKKPVTYLEDSDDDF. Anti-H4K5 antibodies were raised in this study against a peptide of SGRGKGGKGLGKGGAKRHRC where Lysine 5 of the peptide was monoacetylated.

Immunodepletions—To deplete Top2α from *Xenopus* egg extracts, 1.29 volumes Protein A-coupled magnetic beads (Dynabeads Protein A (30 μg/μl)) were bound to anti-Top2α or control IgGs (0.5 μg antibody per 1 μg beads). Antibody-bound beads were then incubated with 1 volume of NPE or 0.5 volumes HSS for 20 minutes at room temperature with end-over-end rotation and this was repeated once. Depleted extracts were then collected and used for DNA replication (as above). For rescue experiments, human Top2α was added at a final concentration of 26.67 ng/μl.

Inhibition and induction of termination—Termination was either induced or blocked using a LacR array as previously described (Dewar et al., 2015). Briefly, 0.05 volumes of plasmid DNA harboring a *lacO* array (300 ng/μl) were incubated with 0.1 volumes LacR (18 μM) at room temperature for 90 minutes. Licensing mix was then prepared by adding 0.85 volumes of HSS supplemented with nocodazole (final concentration: 3ng/μl) and ATP regenerating system (ARS, final concentration: 20mM phosphocreatine, 2 mM ATP, 5 ng/μl creatine phosphokinase). Licensing and initiation of replication were performed as described above. To induce termination, replication proceeded for 12–18 minutes before addition of IPTG to a final concentration of 50 mM.

Replication and Termination assays—DNA synthesis, fork merger, ligation, decatenation, and analysis of DNA topoisomers were performed as previously described (Dewar et al., 2015) and briefly summarized below.

To monitor DNA synthesis, reactions were stopped then treated with RNase A and Proteinase K (as described above) before being separated on a 1% agarose gel at 4 V/cm. Radiolabeled DNA was detected by phosphorimaging to measure incorporation of radio-nucleotides. Total lane signal was quantified using ImageQuant (GE Healthcare) and normalized to the maximum total lane signal across all time points and conditions. Decatenation was quantified from the same gels as the percentage of signal present in the supercoiled monomeric products of replication.

To monitor fork merger, 0.25–1.0 ng/μl purified DNA was digested with 0.4 units/μl XmnI in CutSmart Buffer (NEB) for 1 hour at 37°C. Digested DNA was separated on a 1% agarose gel at 4V/cm. Radiolabeled DNA was detected by phosphorimaging. Fork merger was quantified as the percentage of signal present in the linear molecules.

To monitor ligation, 0.25–1.0 ng/ul purified DNA was digested with 0.4 units/μl AlwNI in CutSmart Buffer (NEB) for 1 hour at 37°. Digested DNA was separated on a 1.5% denaturing alkaline gel at 1.5V/cm. Radiolabeled DNA was detected by phosphorimaging. Ligation was quantified as the percentage of signal present in the fully ligated molecules.

To analyze topoisomers, Top2 treatment was performed on 0.25 ng/μl of purified DNA using 0.2 U/μl human Top2α (Topogen) in Top2α buffer (Topogen) at 37° for 15 minutes. Linearization was performed using 0.4 units/μl XmnI in CutSmart Buffer (NEB) for 1 hour at 37°C. Nicking was performed using 0.04 U/μl Nt.BspQI in Cutsmart buffer (NEB) for 1 hour at 37°C.

2D Gel electrophoresis—To monitor replication intermediates, purified DNA was digested with XmnI (as described above) and then separated on a 0.4% agarose gel at 1 V/cm. The gel was stained with 0.3 μg/ml ethidium bromide then lanes were excised and recast in a 1% gel containing 0.3 μg/ml ethidium bromide before being separated at 4.5V/cm. Radiolabelled DNA was detected by phosphorimaging.

To assess the extent of catenation, purified DNA was digested with 0.04 U/μl Nb.BbvCI and then separated on a 0.4% agarose gel at 0.9 V/cm. The gel was stained with 0.3 μg/ml ethidium bromide then lanes were excised and recast in a 1.2% gel containing 0.3 μg/ml ethidium bromide before being separated at 4.8V/cm. Radiolabeled DNA was detected by phosphorimaging. Catenation was quantified as the percentage total catenane signal within each catenated species. Catenation was plotted as cumulative frequency (‘running total’); for each catenated species, the percent signal was added to the signal from all lesser-catenated species.

Plasmid constructs—For most experiments, p[lacOx16] (pJD152) and p[lacOx32] (pJD156) were used, which were described previously (Dewar et al., 2015). To generate a ladder corresponding to different amounts of unreplicated DNA, p[lacOx4] (pJD82, 3027 bp), p[lacOx8] (pJD85, 3152 bp), p[lacOx12] (pJD104, 3277 bp), and p[lacOx16] (pJD88, 3402 bp) were used and were also described previously (Dewar et al., 2015). pJD34 (p[empty] 2961 bp) is the parental vector, which is pBlueScript II KS(−).

Measurement of nascent strands—To measure the amount of unreplicated DNA in mock- and Top2α-immunodepleted samples, a ladder was generated corresponding to different amounts of unreplicated DNA. To achieve this, p[lacOx16] (3402 bp), p[lacOx12] (3277 bp), p[lacOx8] (3152 bp), p[lacOx4] (3027 bp) and p[empty] (2961 bp) were replicated to completion in the presence of [α-^{32}P]dATP, then digested with XmnI (NEB). In parallel, replication intermediates of p[lacOx16] were purified from mock- or Top2α-immunodepleted extracts, then nicked with 0.4 U/μl BssSI in 3.1 Buffer (NEB) for 1 hour at 37°C. To address the impact of Top2α on product size, the ladder and replication

intermediates were then separated on a 1.5% denaturing alkaline gel at 1.27 V/cm. Radiolabeled DNA was detected by phosphorimaging and quantified using ImageQuant (GE Healthcare) to generate a histogram of the signal within each lane. Peak signal of bands corresponding to the ladder and replication intermediates were manually assigned using the local maximum value. Migration of the ladder was fitted to a 4^{th} order polynomial and used to interpolate the size of replication intermediates.

To measure the size of nascent strands stalled at a LacR array the approach described above was used, with the following modifications. The ladder was generated by end-labeling 1kb DNA ladder (NEB) and 100 bp DNA ladder (NEB) with [$\gamma-^{32}$P]ATP. The ladder was then run alongside replication intermediates of a different p[lacOx16] (pJD152, 3148 bp). Migration of the ladder was fitted to a logarithmic decay and used to interpolate the size of replication intermediates.

End labeling of DNA—To generate radiolabeled DNA ladder, 100 ng/μl DNA was treated with 0.5 U/μl T4 Polynucleotide Kinase (PNK, NEB) in 1X PNK Reaction Buffer (NEB) containing 1.33 μM [$\gamma-^{32}$P]ATP at 37°C for 45 minutes. Radiolabelled DNA was then purified through a Microspin G-50 column (GE Healthcare) according to the manufacturer's instructions.

Nick translation of DNA—To radiolabel parental DNA strands, 8 μl of plasmid DNA (100–150 ng/μl) was added to 1 μl of NEB Buffer 2.1 (10X) and incubated with 1 μl Nb.BbvCI (10 units/μl) at 37°C for 1 hour, followed by heat inactivation at 80°C for 20 minutes. The mix was then supplemented with 0.5 μl NEB Buffer 2.1 (10X), 2.5 μl dNTPs (25 mM each of dCTP, dGTP, dTTP), 1.5 μl *E. coli* DNA Polymerase 1 (10 U/μl), and 0.5 μl [α^{32}P]-dATP (3.33 μM), then incubated at 16°C for 10 minutes. For control unlabeled samples, a parallel reaction was performed where 0.5 μl of unlabeled dATP (3.33 μM) was added. Nick-translated DNA was then buffer exchanged into 10 mM Tris (pH 7.4) using micro Bio-Spin columns (Bio-Rad) and used for replication.

Plasmid pull downs—Plasmid pull downs were performed as previously described (Dewar et al., 2017), but with slight modification to increase the stringency of the DNA binding and wash steps. In brief, 1 volume of Streptavidin-coupled magnetic beads (Dynabeads M-280 Streptavidin, 10 mg/ml) was washed three times with 6 volumes of binding buffer (50 mM Tris-HCl pH 8, 150 mM NaCl, 1mM EDTA, 0.02% Tween 20 (V/V)). Beads were then resuspended in 6 volumes of binding buffer supplemented with 1 pmol biotinylated LacR per 10 mg of beads and incubated for 40 minutes at room temperature with end-over-end rotation. Beads were washed twice with 9 volumes binding buffer, then twice with 9 volumes PPD buffer (20 mM HEPES pH7.7, 500 mM sucrose, 5 mM $MgCl_2$, 100 mM KCl, 0.5 mg/ml BSA, 0.04% Tween (V/V)), before being resuspended in 5 volumes PPD buffer. 15 μl aliquots of resuspended beads were cooled on ice and allowed to settle. For each sample, 3 μl of reaction was withdrawn and added to 15 μl chilled beads, which were resuspended by pipetting up-and-down 40 times immediately after sample addition. Samples were stored on ice until the end of the experiment, then transferred to the cold room. Beads were resuspended by pipetting then incubated for 30 minutes with end-over-end rotation at 4°C. Beads were then pelleted, and the supernatant was removed. Beads

were then washed twice with 400 μl Wash buffer (20 mM HEPES pH7.7, 5 mM $MgCl_2$, 100 mM KCl, 0.25 mg/ml BSA, 0.03% Tween (V/V)) and proteins were eluted with Laemmli Sample buffer. Samples were analyzed by Western Blotting and quantified using ImageJ. To measure replication-dependent protein binding, the signal present in a Cdc7-i control sample was subtracted as background.

Image processing—Exposure (brightness) of autoradiography and western blot images was adjusted to allow all bands to be clearly visible. In most cases this resulted in over-exposure of one or more bands corresponding to abundant species. For any gels where bands were overexposed, an additional image is included in the supplemental data showing a linear exposure (i.e., not overexposed). The only exceptions to this were; 2-D gels, where the 1N spot had to be overexposed to allow replication intermediates to be visualized (Figure S4A); and gels that included radiolabeled molecular weight markers, where the molecular weight markers had to be overexposed in order to see the data bands (Figures S4C, S4D, and S3H). All image processing was performed evenly across the entire image. Contrast was never adjusted and background was never subtracted from the display images.

QUANTIFICATION AND STATISTICAL ANALYSIS

Quantification—Autoradiographs were quantified using ImageQuant TL (GE Healthcare). All quantification was performed on original unprocessed images.

Statistical Analysis—Where multiple experiments were summarized as a single graph, the mean of all experiments is plotted and error bars indicate standard deviation (SD). In these cases, n is indicated in the figure legend and represents the number of independently assembled reactions, which constitute biological replicates.

DATA AND CODE AVAILABILITY

This study did not analyze or generate any datasets or code.

Supplementary Material

Refer to Web version on PubMed Central for supplementary material.

ACKNOWLEDGMENTS

J.M.D. was supported by NIH grant R35GM128696 and ACS grant IRG-15-169-56. N.O. was supported by NIH grant R01GM126363. We thank Jon Baxter, David Cortez, Houra Merrikh, and Jared Nordman for valuable feedback on the manuscript. We also thank Sabrina Van Ravenstein and Jesus Mallol Diaz for experimental assistance.

REFERENCES

Baxter J, and Diffley JF (2008). Topoisomerase II inactivation prevents the completion of DNA replication in budding yeast. Mol. Cell 30, 790–802. [PubMed: 18570880]

Bell SP, and Labib K (2016). Chromosome Duplication in Saccharomyces cerevisiae. Genetics 203, 1027–1067. [PubMed: 27384026]

Bermejo R, Doksani Y, Capra T, Katou YM, Tanaka H, Shirahige K, and Foiani M (2007). Top1- and Top2-mediated topological transitions at replication forks ensure fork progression and stability and prevent DNA damage checkpoint activation. Genes Dev. 21, 1921–1936. [PubMed: 17671091]

Bleichert F, Botchan MR, and Berger JM (2017). Mechanisms for initiating cellular DNA replication. Science 355, eaah6317. [PubMed: 28209641]

Brill SJ, DiNardo S, Voelkel-Meiman K, and Sternglanz R (1987). Need for DNA topoisomerase activity as a swivel for DNA replication for transcription of ribosomal RNA. Nature 326, 414–416. [PubMed: 2436053]

Bromberg KD, Hendricks C, Burgin AB, and Osheroff N (2002). Human topoisomerase IIalpha possesses an intrinsic nucleic acid specificity for DNA ligation. Use of 50 covalently activated oligonucleotide substrates to study enzyme mechanism. J. Biol. Chem 277, 31201–31206. [PubMed: 12050172]

Champoux JJ, and Been MD (1980). Mechanistic Studies of DNA Replication and Genetic Recombination In ICN-UCLA Symposia on Molecular and Cellular Biology, Albert B, ed. (New York Academic Press), pp. 809–815.

Cuvier O, Stanojcic S, Lemaitre JM, and Mechali M (2008). A topoisomerase II-dependent mechanism for resetting replicons at the S-M-phase transition. Genes Dev 22, 860–865. [PubMed: 18381889]

Deegan TD, Baxter J, Ortiz Bazan MA, Yeeles JTP, and Labib KPM (2019). Pif1-Family Helicases Support Fork Convergence during DNA Replication Termination in Eukaryotes. Mol. Cell 74, 231–244.e9. [PubMed: 30850330]

Deng L, Wu RA, Kochenova OV, Pellman DS, and Walter JC (2018). Mitotic CDK promotes replisome disassembly, fork breakage, and complex DNA rearrangements. Mol. Cell 73, 915–929.e6.

Dewar JM, and Walter JC (2017). Mechanisms of DNA replication termination. Nat. Rev. Mol. Cell Biol 18, 507–516. [PubMed: 28537574]

Dewar JM, Budzowska M, and Walter JC (2015). The mechanism of DNA replication termination in vertebrates. Nature 525, 345–350. [PubMed: 26322582]

Dewar JM, Low E, Mann M, Räschle M, and Walter JC (2017). $CRL2^{Lrr1}$ promotes unloading of the vertebrate replisome from chromatin during replication termination. Genes Dev 31, 275–290. [PubMed: 28235849]

Elsea SH, Hsiung Y, Nitiss JL, and Osheroff N (1995). A yeast type II topoisomerase selected for resistance to quinolones. Mutation of histidine 1012 to tyrosine confers resistance to nonintercalative drugs but hypersensitivity to ellipticine. J. Biol. Chem 270, 1913–1920. [PubMed: 7829529]

Espeli O, Levine C, Hassing H, and Marians KJ (2003). Temporal regulation of topoisomerase IV activity in E. coli. Mol. Cell 11, 189–201. [PubMed: 12535532]

Gaggioli V, Le Viet B, Germe T, and Hyrien O (2013). DNA topoisomerase IIα controls replication origin cluster licensing and firing time in Xenopus egg extracts. Nucleic Acids Res 41, 7313–7331. [PubMed: 23757188]

Gambus A (2017). Termination of Eukaryotic Replication Forks. Adv. Exp. Med. Biol 1042, 163–187. [PubMed: 29357058]

Gardner L, Malik R, Shimizu Y, Mullins N, and ElShamy WM (2011). Geminin overexpression prevents the completion of topoisomerase IIα chromosome decatenation, leading to aneuploidy in human mammary epithelial cells. Breast Cancer Res 13, R53. [PubMed: 21595939]

Hiasa H, and Marians KJ (1994). Tus prevents overreplication of oriC plasmid DNA. J. Biol. Chem 269, 26959–26968. [PubMed: 7929435]

Hiasa H, and Marians KJ (1996). Two distinct modes of strand unlinking during theta-type DNA replication. J. Biol. Chem 271, 21529–21535. [PubMed: 8702938]

Huberman JA, and Riggs AD (1968). On the mechanism of DNA replication in mammalian chromosomes. J. Mol. Biol 32, 327–341. [PubMed: 5689363]

Ishimi Y, Sugasawa K, Hanaoka F, Eki T, and Hurwitz J (1992). Topoisomerase II plays an essential role as a swivelase in the late stage of SV40 chromosome replication in vitro. J. Biol. Chem 267, 462–466. [PubMed: 1309747]

Ivessa AS, Zhou JQ, and Zakian VA (2000). The Saccharomyces Pif1p DNA helicase and the highly related Rrm3p have opposite effects on replication fork progression in ribosomal DNA. Cell 100, 479–489. [PubMed: 10693764]

Keszthelyi A, Minchell NE, and Baxter J (2016). The Causes and Consequences of Topological Stress during DNA Replication. Genes (Basel) 7, E134. [PubMed: 28009828]

Kingma PS, Greider CA, and Osheroff N (1997). Spontaneous DNA lesions poison human topoisomerase IIalpha and stimulate cleavage proximal to leukemic 11q23 chromosomal breakpoints. Biochemistry 36, 5934–5939. [PubMed: 9166762]

Kochaniak AB, Habuchi S, Loparo JJ, Chang DJ, Cimprich KA, Walter JC, and van Oijen AM (2009). Proliferating cell nuclear antigen uses two distinct modes to move along DNA. J. Biol. Chem 284, 17700–17710. [PubMed: 19411704]

Lebofsky R, Takahashi T, and Walter JC (2009). DNA replication in nucleus-free Xenopus egg extracts. Methods Mol. Biol 521, 229–252. [PubMed: 19563110]

Lee CM, Wang G, Pertsinidis A, and Marians KJ (2019). Topoisomerase III Acts at the Replication Fork to Remove Precatenanes. J. Bacteriol 201, e00563–18. [PubMed: 30617245]

Lucas I, Germe T, Chevrier-Miller M, and Hyrien O (2001). Topoisomerase II can unlink replicating DNA by precatenane removal. EMBO J 20, 6509–6519. [PubMed: 11707421]

Maric M, Maculins T, De Piccoli G, and Labib K (2014). Cdc48 and a ubiquitin ligase drive disassembly of the CMG helicase at the end of DNA replication. Science 346, 1253596. [PubMed: 25342810]

Mariezcurrena A, and Uhlmann F (2017). Observation of DNA intertwining along authentic budding yeast chromosomes. Genes Dev 31, 2151–2161. [PubMed: 29208645]

McClendon AK, Rodriguez AC, and Osheroff N (2005). Human topoisomerase IIalpha rapidly relaxes positively supercoiled DNA: implications for enzyme action ahead of replication forks. J. Biol. Chem 280, 39337–39345. [PubMed: 16188892]

McGarry TJ, and Kirschner MW (1998). Geminin, an inhibitor of DNA replication, is degraded during mitosis. Cell 93, 1043–1053. [PubMed: 9635433]

Mimura S, and Takisawa H (1998). Xenopus Cdc45-dependent loading of DNA polymerase alpha onto chromatin under the control of S-phase Cdk. EMBO J 17, 5699–5707. [PubMed: 9755170]

Montagnoli A, Valsasina B, Croci V, Menichincheri M, Rainoldi S, Marchesi V, Tibolla M, Tenca P, Brotherton D, Albanese C, et al. (2008). A Cdc7 kinase inhibitor restricts initiation of DNA replication and has antitumor activity. Nat. Chem. Biol 4, 357–365. [PubMed: 18469809]

Moreno SP, Bailey R, Campion N, Herron S, and Gambus A (2014). Polyubiquitylation drives replisome disassembly at the termination of DNA replication. Science 346, 477–481. [PubMed: 25342805]

Nitiss JL (2009). Targeting DNA topoisomerase II in cancer chemotherapy. Nat. Rev. Cancer 9, 338–350. [PubMed: 19377506]

O'Donnell M, Langston L, and Stillman B (2013). Principles and concepts of DNA replication in bacteria, archaea, and eukarya. Cold Spring Harb. Perspect. Biol 5, a010108.

Pommier Y, Sun Y, Huang SN, and Nitiss JL (2016). Roles of eukaryotic topoisomerases in transcription, replication and genomic stability. Nat. Rev. Mol. Cell Biol 17, 703–721. [PubMed: 27649880]

Ray Chaudhuri A, Hashimoto Y, Herrador R, Neelsen KJ, Fachinetti D, Bermejo R, Cocito A, Costanzo V, and Lopes M (2012). Topoisomerase I poisoning results in PARP-mediated replication fork reversal. Nat. Struct. Mol. Biol 19, 417–423. [PubMed: 22388737]

Roca J, Ishida R, Berger JM, Andoh T, and Wang JC (1994). Antitumor bisdioxopiperazines inhibit yeast DNA topoisomerase II by trapping the enzyme in the form of a closed protein clamp. Proc. Natl. Acad. Sci. USA 91, 1781–1785. [PubMed: 8127881]

Rowley MJ, and Corces VG (2018). Organizational principles of 3D genome architecture. Nat. Rev. Genet 19, 789–800. [PubMed: 30367165]

Rudolph CJ, Upton AL, Stockum A, Nieduszynski CA, and Lloyd RG (2013).Avoiding chromosome pathology when replication forks collide. Nature 500, 608–611. [PubMed: 23892781]

Schalbetter SA, Mansoubi S, Chambers AL, Downs JA, and Baxter J (2015). Fork rotation and DNA precatenation are restricted during DNA replication to prevent chromosomal instability. Proc. Natl. Acad. Sci. USA 112, E4565–E4570. [PubMed: 26240319]

Seidman MM, and Salzman NP (1979). Late replicative intermediates are accumulated during simian virus 40 DNA replication in vivo and in vitro. J. Virol 30, 600–609. [PubMed: 224218]

Semlow DR, Zhang J, Budzowska M, Drohat AC, and Walter JC (2016). Replication-Dependent Unhooking of DNA Interstrand Cross-Links by the NEIL3 Glycosylase. Cell 167, 498–511.e14. [PubMed: 27693351]

Siddiqui K, On KF, and Diffley JF (2013). Regulating DNA replication in eukarya. Cold Spring Harb. Perspect. Biol 5, a012930. [PubMed: 23838438]

Sonneville R, Moreno SP, Knebel A, Johnson C, Hastie CJ, Gartner A, Gambus A, and Labib K (2017). CUL-2^{LRR-1} and UBXN-3 drive replisome disassembly during DNA replication termination and mitosis. Nat. Cell Biol 19, 468–479. [PubMed: 28368371]

Sparks JL, Chistol G, Gao AO, Räschle M, Larsen NB, Mann M, Duxin JP, and Walter JC (2019). The CMG Helicase Bypasses DNA-Protein Cross-Links to Facilitate Their Repair. Cell 176, 167–181.e21. [PubMed: 30595447]

Suski C, and Marians KJ (2008). Resolution of converging replication forks by RecQ and topoisomerase III. Mol. Cell 30, 779–789. [PubMed: 18570879]

Tapper DP, and DePamphilis ML (1978). Discontinuous DNA replication: accumulation of Simian virus 40 DNA at specific stages in its replication. J. Mol. Biol 120, 401–422. [PubMed: 206700]

Ullsperger CJ, Vologodskii AV, and Cozzarelli NR (1995). Unlinking of DNA by Topoisomerases During DNA Replication. Nucleic Acids Mol. Biol 9, 115–142.

Vos SM,Tretter EM, Schmidt BH, and Berger JM (2011). All tangled up: how cells direct, manage and exploit topoisomerase function. Nat. Rev. Mol. Cell Biol 12, 827–841. [PubMed: 22108601]

Walter J, and Newport J (2000). Initiation of eukaryotic DNA replication: origin unwinding and sequential chromatin association of Cdc45, RPA, and DNA polymerase alpha. Mol. Cell 5, 617–627. [PubMed: 10882098]

Walter J, Sun L, and Newport J (1998). Regulated chromosomal DNA replication in the absence of a nucleus. Mol. Cell 1, 519–529. [PubMed: 9660936]

Wang WL, and Shechter D (2016). Chromatin assembly and transcriptional cross-talk in Xenopus laevis oocyte and egg extracts. Int. J. Dev. Biol 60, 315–320. [PubMed: 27759158]

Wohlschlegel JA, Dwyer BT, Dhar SK, Cvetic C, Walter JC, and Dutta A (2000). Inhibition of eukaryotic DNA replication by geminin binding to Cdt1. Science 290, 2309–2312. [PubMed: 11125146]

Worland ST, and Wang JC (1989). Inducible overexpression, purification, and active site mapping of DNA topoisomerase II from the yeast Saccharomyces cerevisiae. J. Biol. Chem 264, 4412–4416. [PubMed: 2538443]

Wu RA, Semlow DR, Kamimae-Lanning AN, Kochenova OV, Chistol G, Hodskinson MR, Amunugama R, Sparks JL, Wang M, Deng L, et al. (2019). TRAIP is a master regulator of DNA interstrand crosslink repair. Nature 567, 267–272. [PubMed: 30842657]

Wühr M, Güttler T, Peshkin L, McAlister GC, Sonnett M, Ishihara K, Groen AC, Presler M, Erickson BK, Mitchison TJ, et al. (2015). The Nuclear Proteome of a Vertebrate. Curr. Biol 25, 2663–2671. [PubMed: 26441354]

Yeeles JT, Deegan TD, Janska A, Early A, and Diffley JF (2015). Regulated eukaryotic DNA replication origin firing with purified proteins. Nature 519, 431–435. [PubMed: 25739503]

Highlights

- Top2α is crucial for fork convergence in *Xenopus* egg extracts
- Fork merger can occur slowly through Top2α-independent mechanisms
- Loss of Top2α causes converging forks to stall ~300 bp apart
- Top2α promotes fork convergence by acting throughout replication

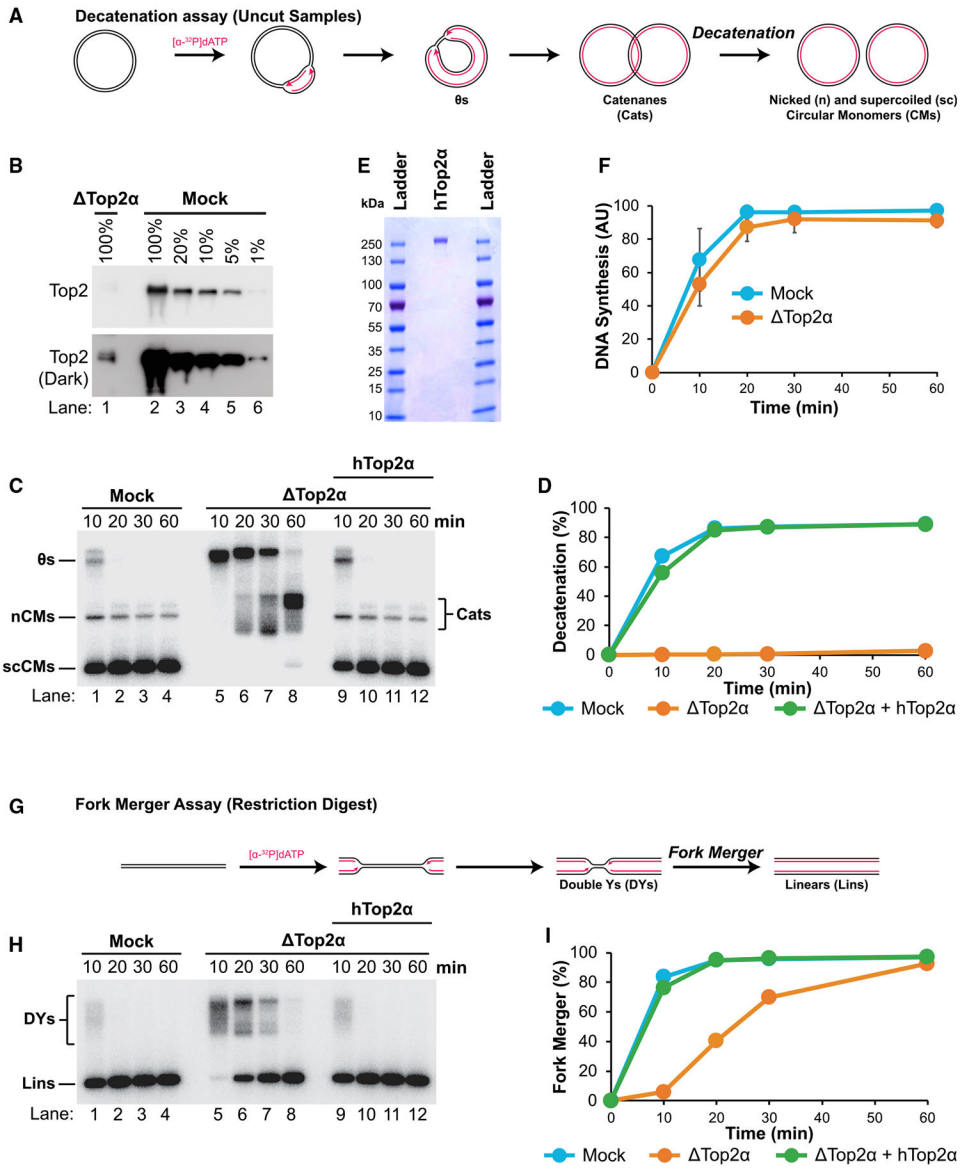

Figure 1. Top2α Is Important for Decatenation and Fork Merger

(A) Schematic of the decatenation assay.

(B) Top2α-immunodepleted extracts were visualized alongside mock-immunodepleted extracts by western blotting. The dark panel is overexposed.

(C) Plasmid DNA was replicated in mock-, Top2α-immunodepleted, and rescued (ΔTop2α +hTop2α) extracts containing [α−^{32}P]dATP. Replication intermediates were purified and then separated on an agarose gel and visualized by autoradiography. See also Figures S1E–S1G and S1B.

(D) Quantification of decatenation in (C). See also Figure S1C.

(E) 500 ng of human Top2α was separated on a polyacrylamide gel and visualized by Coomassie staining.

(F) DNA synthesis was measured during plasmid DNA replication in mock- and Top2α-immunodepleted extracts. Plot depicts mean ± SD from 4 experiments.

(G) Schematic of the fork merger assay.
(H) DNA samples from (E) were digested and then separated on an agarose gel and visualized by autoradiography. See also Figure S1H.
(I) Quantification of fork merger in (H). See also Figure S1I.

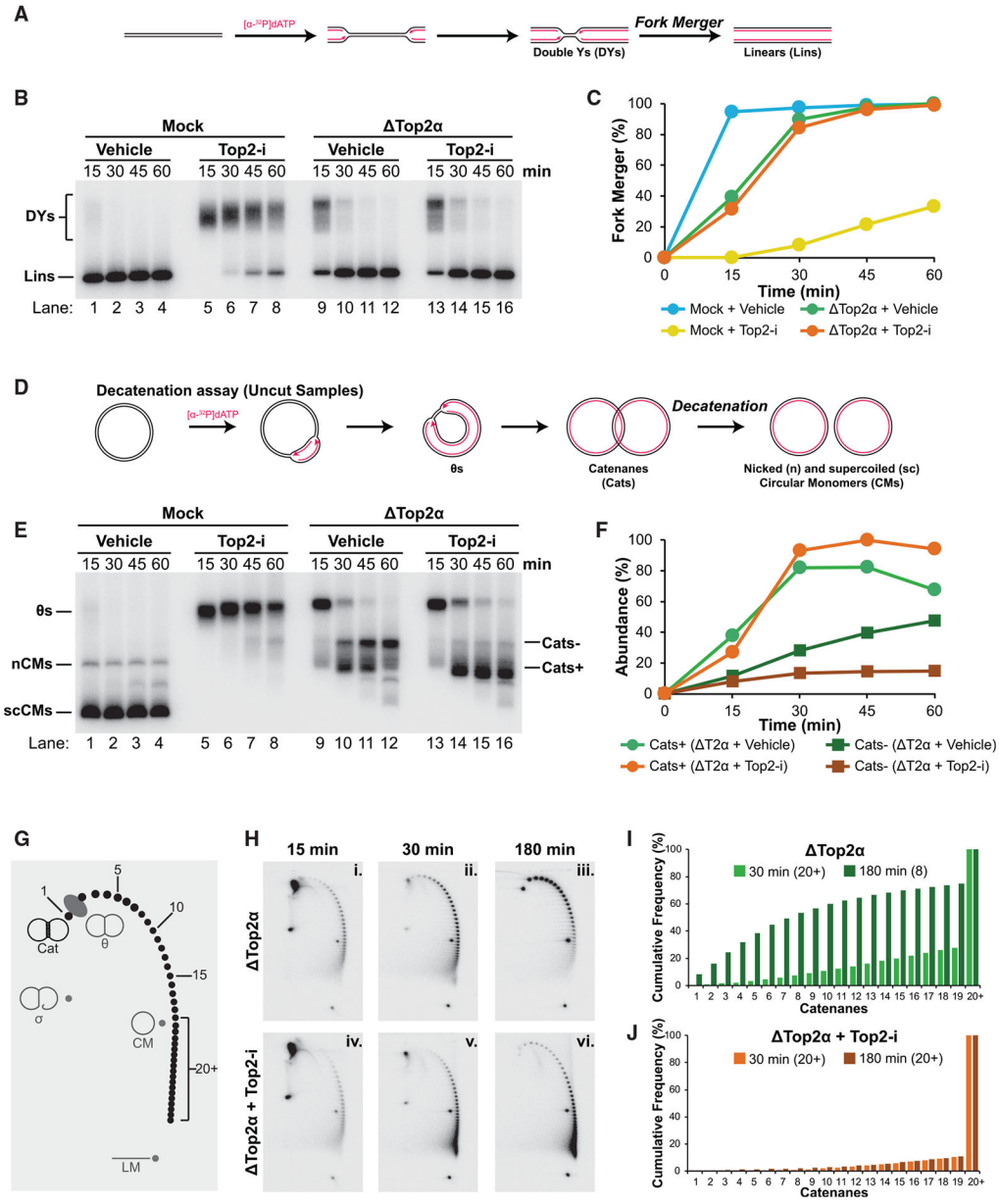

Figure 2. Fork Merger, but Not Decatenation, Can Occur in the Absence of Top2α

(A) Schematic of the fork merger assay.

(B) Plasmid DNA replication was performed in mock- or Top2α-immunodepleted extracts containing [α−^{32}P]dATP and either vehicle or Top2-i. Replication intermediates were purified, digested, and then separated on an agarose gel and visualized by autoradiography. See also Figure S2A.

(C) Quantification of fork merger in (B). See also Figure S2B.

(D) Schematic of the decatenation assay.

(E) Replication intermediates from (B) were separated on an agarose gel and visualized by autoradiography. See also Figure S2G.

(F) Quantification of Cats− and Cats+ in (E). See also Figures S2I–S2K.

(G) Schematic of DNA structures observed by 2D gel analysis of nicked replication intermediates. The source of the θs, Cats, and cm is indicated in (D). Linear monomers (LMs) arise from a double-strand breaks in cm, while σs arise from double-strand breaks in θs. Each catenated species runs at a discrete location corresponding to the number of catenanes present. Numbers indicate how many catenated linkages are present.

(H) Plasmid DNA was replicated in Top2α-immunodepleted extracts containing [α $-^{32}$P]dATP and either Vehicle or Top2-i. Replication intermediates were purified, nicked, and then separated by 2D gel electrophoresis and detected by autoradiography. See also Figure S3J.

(I and J) Quantification of the number of catenanes present in the catenanted species detected in (Hii), (Hiii), (Hv), and (Hvi). The graphs depict cumulative frequency distribution, and numbers in parentheses indicate the median number of catenanes in each condition. See also Figures S3K–S3N.

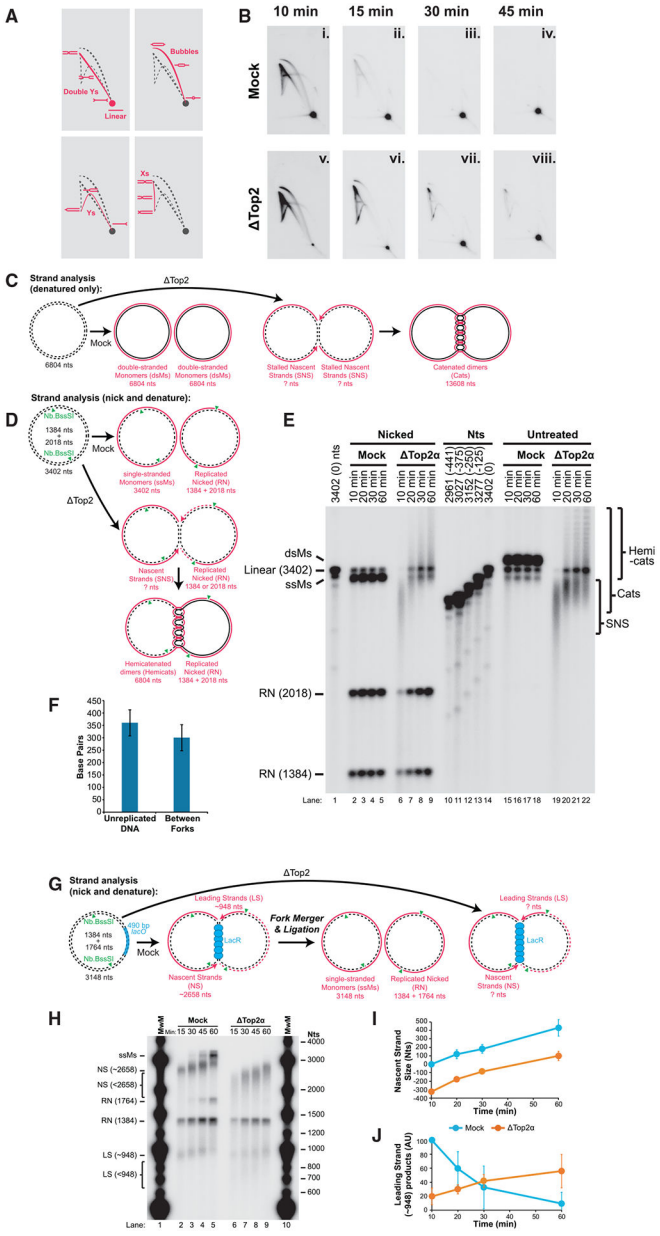

Figure 3. Loss of Top2α Impairs Fork Convergence

(A) Schematic of DNA structures observed by 2D gel electrophoresis following restriction digest (as in Figure 1G). Double Ys and Xs arise from intermediates cut behind two forks, while bubbles occur when intermediates are cut between two forks. Ys arise from incision of one fork (see Figure S4B).

(B) Plasmid DNA was replicated in mock- and Top2α-immunodepleted extracts containing [α–^{32}P] dATP. To monitor the DNA structures formed, replication intermediates were digested and then separated by 2D gel electrophoresis and detected by autoradiography. See also Figure S4A.

(C) Plasmid DNA was replicated in Mock- and Top2α-immunodepleted extracts containing [α–^{32}P] dATP. Replication intermediates were purified then denatured. The expected

products are shown. Black lines indicate unlabeled parental strands. Dashed lines represent strands that should not be detectable because they are unlabeled or not intertwined with a labeled strand.

(D) Schematic depicting the effect of Nb.BssSI treatment on the intermediates shown in (C).

(E) Replication intermediates from (C) and (D) were separated on a denaturing agarose gel and visualized by autoradiography. Structures indicated in (C) and (D) are labeled. Linear (3,402) molecules arise from double-stranded monomers that were nicked during DNA purification, prior to Nb.BssSI treatment. Lanes 10–14 are molecular weight standards of the indicated sizes. The numbers in parentheses represent the amount of unreplicated DNA in lanes 2–9 and 15–22 that each standard corresponds to. See also Figures S4C and S4H–S4K.

(F) Quantification of the amount of unreplicated DNA in lane 6 of (E) after correcting for the ~60-bp footprint of the replisome (Dewar et al., 2015). Plot depicts mean ± SD from 4 experiments.

(G) Plasmid DNA containing a LacR-bound 16x*lacO* array was replicated in mock- and Top2α-immunodepleted extracts containing [α^{-32}P]dATP. Replication intermediates were purified and then nicked and denatured.

(H) Replication intermediates from (G) were separated on a denaturing agarose gel alongside a DNA ladder. Note that lanes 1 and 10 are overexposed. See also Figures S4L–S4Q.

(I) Quantification of the size of the nascent strand products from (H) relative to the initial size of the nascent products in mock-immunodepleted extracts. Plot depicts mean ± SD from 3 experiments.

(J) Quantification of the abundance of the leading strand (~948) products from (H) relative to the initial abundance in mock-immunodepleted extracts. Plot depicts mean ± SD from 3 experiments.

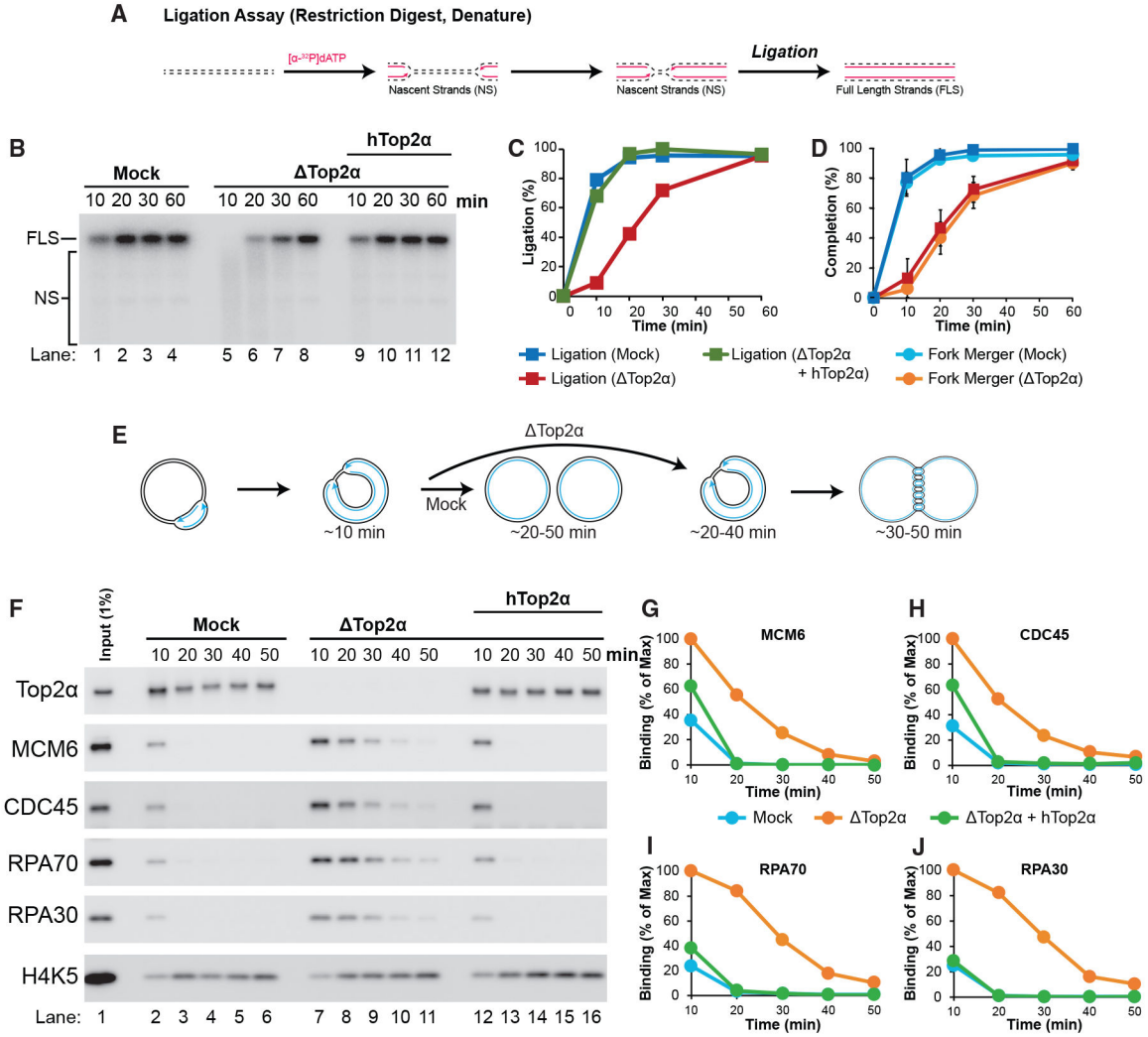

Figure 4. Top2α Is Crucial for Ligation and Replisome Unloading

(A) Schematic of the ligation assay. Dashed lines represent unlabeled parental strands, which are not detected.

(B) Plasmid DNA was replicated in mock-, Top2α-immunodepleted, and rescued (ΔTop2α +hTop2α) extracts containing [α–^{32}P]dATP. Replication intermediates were purified, digested, and then separated on a denaturing agarose gel and visualized by autoradiography. See also Figure S5A.

(C) Quantification of ligation in (B). See also Figure S5B.

(D) Fork merger and ligation were quantified from multiple experiments. Plot depicts mean ± SD from 4 experiments. See also Figure 1F.

(E) Plasmid DNA replication was performed in mock- and Top2α-immunodepleted extracts, and chromatin-bound proteins were recovered at different time points by plasmid pull-down. Approximate kinetics of DNA replication are indicated.

(F) Chromatin associated proteins from (E) were detected by western blotting.

(G–J) Binding of MCM6 (G), CDC45 (H), RPA70 (I), and RPA30 (J) to chromatin was quantified from (F). See also Figures S5C–S5H.

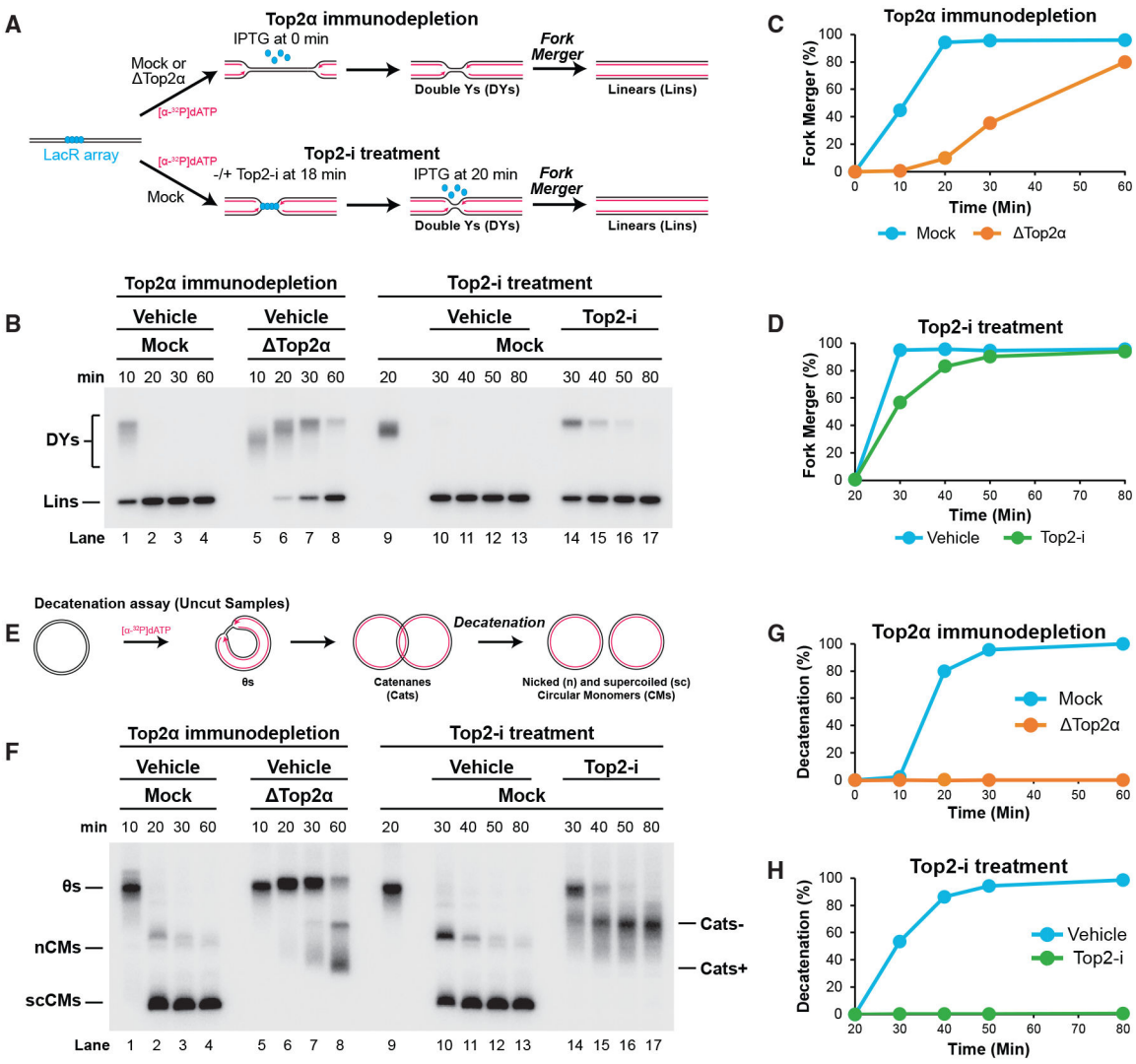

Figure 5. Top2α Acts throughout Replication to Promote Termination

(A) Plasmid DNA containing a LacR-bound 32x*lacO* array was replicated in mock- and Top2α-immunodepleted extracts. To monitor the effect of Top2α loss throughout replication, IPTG was added at the onset of replication to mock- and Top2α-immunodepleted extracts to allow termination to occur (upper panels). To monitor the effect of Top2α loss during termination, replication proceeded in mock-immunodepleted extracts until forks stalled at the LacR array (18 min), then Top2-i was added, and termination was induced by IPTG addition (20 min, lower panels).

(B) Replication intermediates from (A) were purified, digested, and then separated on an agarose gel and visualized by autoradiography. See also Figure S6P.

(C and D) Quantification of fork merger in (B). See also Figures S6Q and S6R.

(E) Schematic of the decatenation assay.

(F) Replication intermediates from (E) were separated on an agarose gel and visualized by autoradiography. See also Figure S6S.

(G and H) Quantification of decatenation in (F). See also Figures S6T and S6U.

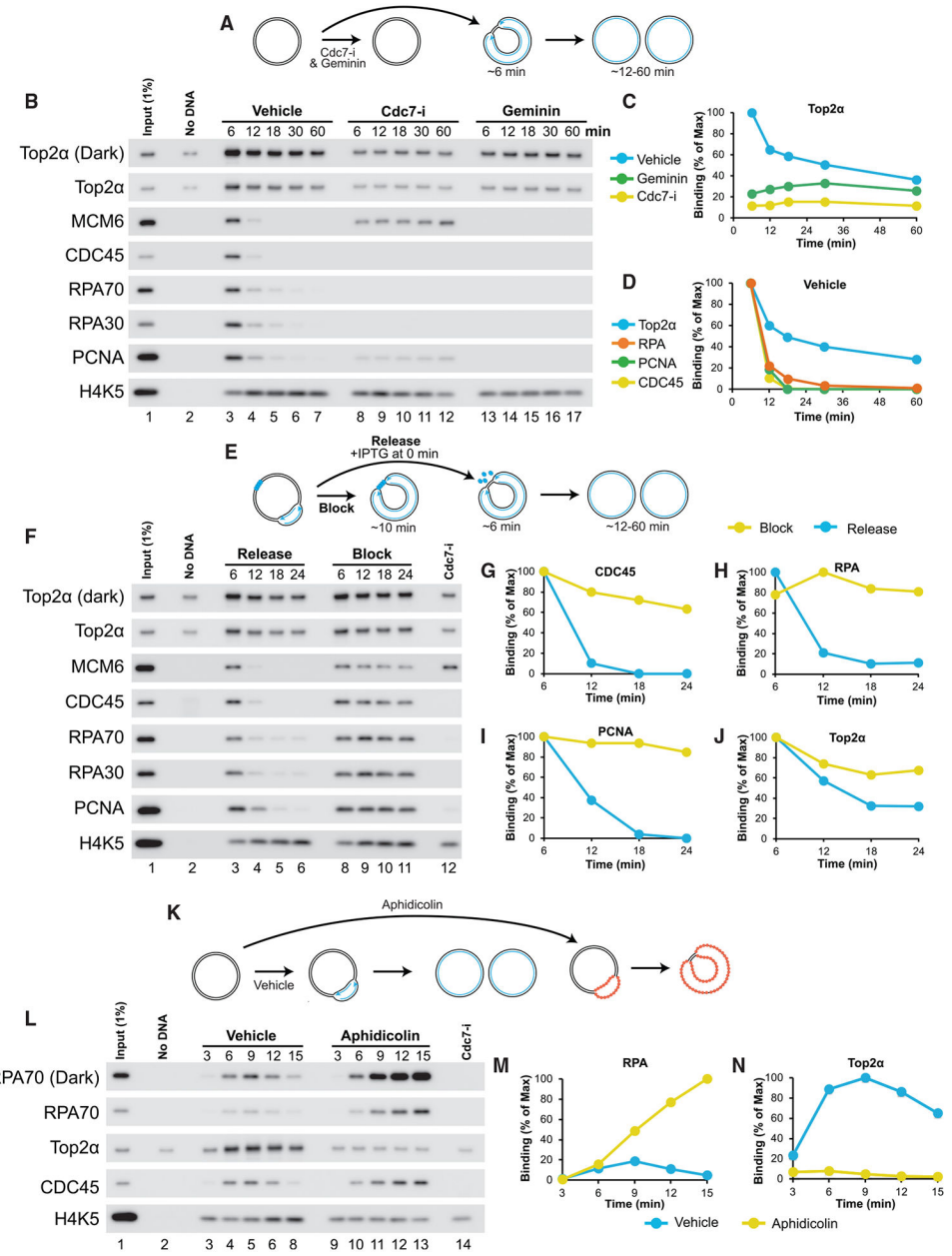

Figure 6. Top2α Binds Pre-catenanes throughout Replication

(A) Plasmid DNA was replicated in extracts treated with vehicle, Cdc7-I, or Geminin. Chromatin-bound proteins were recovered at different time points by plasmid pull-down. Approximate kinetics of DNA replication are indicated.

(B) Chromatin-associated proteins from (A) were detected by western blotting

(C) Binding of Top2α was quantified from (B). See also Figure S7A.

(D) Replication-dependent binding of Top2α, RPA, PCNA, and CDC45 was quantified from (B). See also Figure S7B.

(E) Plasmid DNA containing a LacR-bound 16x*lacO* array was replicated with IPTG added to allow termination ("Release") or omitted to block termination ("Block"). Chromatin-

bound proteins were recovered at different time points by plasmid pull-down. Approximate kinetics of DNA replication are indicated.

(F) Chromatin-associated proteins from (E) were detected by western blotting.

(G–J) Quantification of replication-dependent CDC45 (G), RPA (H), PCNA (I), and Top2α binding in (F). See also Figures S7C–S7I.

(K) Plasmid DNA was replicated in extracts treated with vehicle or aphidicolin. Chromatin-bound proteins were recovered at different time points by plasmid pull-down. Red dots indicate RPA binding to nascent single-stranded DNA in aphidicolin-treated extracts.

(L) Chromatin-associated proteins from (K) were detected by western blotting.

(M and N) Quantification of RPA70 and Top2α binding in (L). See also Figures S7O–S7R.

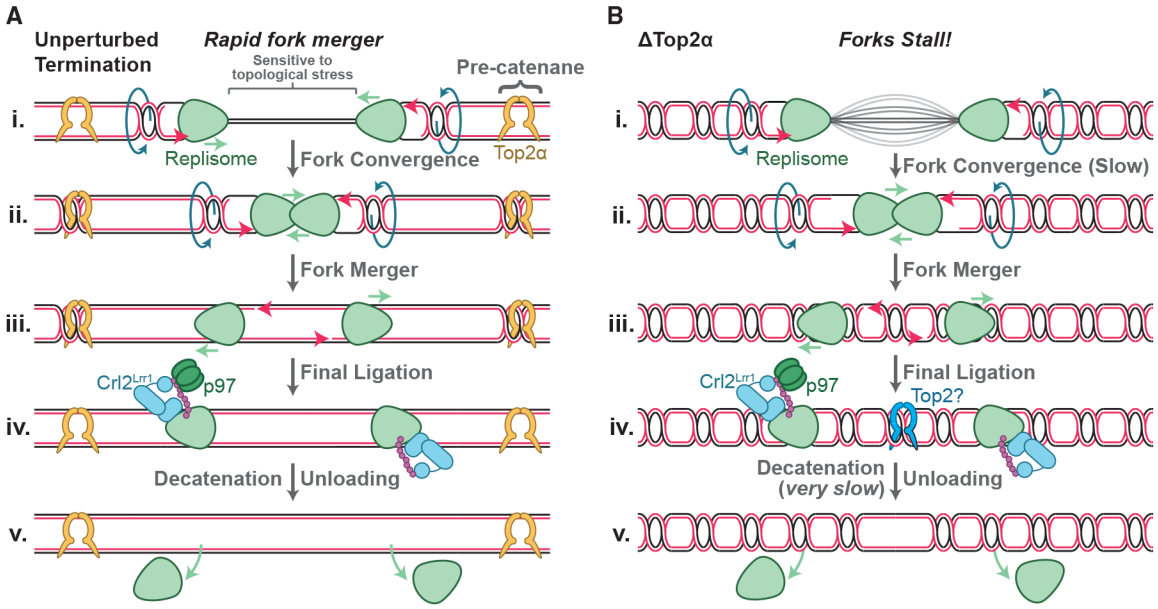

Figure 7. Model for the Role of Top2α during Vertebrate Termination

(A) Under unperturbed conditions, pre-catenanes form prior to termination and are resolved by Top2α to facilitate fork convergence (i). Fork convergence occurs when the final stretch of DNA is unwound, and this process is sensitive to topological stress (i and ii). Once replisomes meet, fork merger, final ligation, replisome unloading, and decatenation proceed rapidly (ii–v) as previously described (Dewar et al., 2015). Top2α binds prior to termination and remains bound throughout this process.

(B) In the absence of Top2α, converging replisomes stall with unreplicated DNA between them due to accumulation of topological stress (i). Fork convergence ultimately goes to completion independently of Top2 activity (i and ii), allowing fork merger (ii and iii), ligation (iii and iv), and replisome unloading (iv and v) to occur, likely through the previously described mechanism for termination. Decatenation occurs very slowly (iv and v) using a different Top2 activity (Top2?) that is likely Top2β.

KEY RESOURCES TABLE

REAGENT or RESOURCE	SOURCE	IDENTIFIER
Antibodies		
Rabbit polyclonal anti-Top2α	This Study	NEP4061
Rabbit polyclonal anti-MCM6	Semlow et al., 2016	NEP2926
Rabbit polyclonal anti-CDC45	Mimura and Takisawa, 1998	N/A
Rabbit polyclonal anti-RPA	Walter and Newport, 2000	N/A
Rabbit polyclonal anti-H4K5	This Study	NEP3893
Rabbit polyclonal anti-PCNA	Kochaniak et al., 2009	N/A
Bacterial and Virus Strains		
E. coli T7 express	New England Biolabs	C2566
E. coli NEB 5-alpha	New England Biolabs	C2987
S. *cerevisiae* Matα ade1–100 leu2–3 leu2–112 ura3–52	Worland and Wang, 1989	DBY745
Chemicals, Peptides, and Recombinant Proteins		
Geminin	McGarry and Kirschner, 1998	N/A
LacR-biotin	Dewar et al., 2015	N/A
ICRF-193	Sigma	I4659
Merbarone	Sigma	445800
PHA-767491	Sigma	PZ0178
IPTG	Invitrogen	15529019
hTop2α	Elsea et al., 1995	N/A
hTop2α-Y805F (hTop2α-YF)	Bromberg et al., 2002	N/A
Proteinase K, recombinant	Roche	RPROTK-RO
RNase A, recombinant	Sigma	R4642
Glycogen	Roche	10901393001
[α−^{32}P]dATP	Perkin Elmer	BLU512Z250UC
[γ−^{32}P]ATP	Perkin Elmer	BLU502Z250UC
Dynabeads Protein A	Invitrogen	10001D
Dynabeads M280 Streptavidin	Invitrogen	11205D
hTop2a (Topogen)	Topogen	TG2000H-1
AlwNI	New England Biolabs	R0514
XmnI	New England Biolabs	R0194
Nt.BspQI	New England Biolabs	R0644
Nb.BssSI	New England Biolabs	R0681
Biotin	Sigma	B4501
T4 Polynucleotide Kinase	New England Biolabs	M0201
ATP	Sigma	A7699
BSA	Sigma	A7906
Phosphocreatine	Sigma	P7936
DTT	Bio-Rad	1610611
Creatine PhosphoKinase (CPK)	Sigma	C3755
HCG	Sigma	CG10

REAGENT or RESOURCE	SOURCE	IDENTIFIER
cOmplete protease inhibitor	Roche	CO-RO
Softlink resin	Promega	V2011
Experimental Models: Organisms/Strains		
Xenopus laevis (females)	Nasco	LM0053MX
Xenopus laevis (males)	Nasco	LM00715MX
Recombinant DNA		
p[lacOx16]	Dewar et al., 2015	pJD152
p[lacOx32]	Dewar et al., 2015	pJD156
p[empty]	Agilent	pBlueScript II KS(−)
p[lacOx4]	Dewar et al., 2015	pJD82
p[lacOx8]	Dewar et al., 2015	pJD85
p[lacOx12]	Dewar et al., 2015	pJD104
p[lacOx16]	Dewar et al., 2015	pJD88
pBirACM	Avidity	AVB99
pET11a[LacR-Avi]	Dewar et al., 2015	pJD72
YEpTOP2-pGAL1	Worland and Wang, 1989	YEpWOB6
YEpTOP2Y805F-pGAL1	Bromberg et al., 2002	N/A
Software and Algorithms		
ImageQuant TL	GE Healthcare	v8.2.0.0